19. OXYGEN AND CARBON ISOTOPE STRATIGRAPHY AT SITE 723, OMAN MARGIN[1]

Nobuaki Niitsuma,[2] Tadamichi Oba,[3] and Makoto Okada[4]

ABSTRACT

Site 723 is located in a water depth of 808 m at the center of the oxygen minimum zone and the middle part of the main thermocline on the Oman Margin.

Oxygen isotope curves of planktonic $\delta^{18}O_P$ and benthic $\delta^{18}O_B$ can be traced back continuously to Stage 23 with high resolution measurements. A tentative correlation to Stage 53 has been tried using oxygen isotope stratigraphy. The amplitudes of the fluctuations of the benthic $\delta^{18}O_B$ curve are small, compared with the planktonic $\delta^{18}O_P$ curve. The delays of benthic oxygen isotopes $\delta^{18}O_B$ related to the planktonic $\delta^{18}O_P$ appear in the transgressive stages.

Carbon isotopes of benthic $\delta^{13}C_B$ and planktonic $\delta^{13}C_P$ generally show an inverse correlation with oxygen isotope values $\delta^{18}O_B$ and $\delta^{18}O_P$, however, the changes of $\delta^{13}C$ are more gradual than those of $\delta^{18}O$ during transgressive stages in spite of the synchronized changes of $\delta^{13}C$ with those of $\delta^{18}O$ during regressive stages.

The difference of oxygen isotope between benthic and planktonic foraminifers represents the degree of pushing up the thermocline by upwelling, and the difference of carbon isotope represents the relative amount of upwelling ΣCO_2 to the biological uptake in the surface water. These isotopic differences can be used as indicators of upwelling and show strong upwelling in the interglacial and weak upwelling in the glacial stages. The organic carbon content is correlated with the isotopic upwelling indicators, and higher content is correlated with the isotopic upwelling indicators and higher content appears in the interglacial stages.

The calculated rate of sedimentation based on oxygen isotope stratigraphy in glacial stages is significantly high, two to four times that of interglacial stages, and the absolute flux of fluvial sediments with variability of lithofacies increased in the glacial stage.

The present glacial-interglacial cycle with the fluctuation of upwelling relating to the southwest monsoon can be traced back to Stage 8, 250 ka. From Stage 8 to 12, 250–450 ka, the upwelling indicator of oxygen isotope difference did not show such distinct cyclicity. For Stages 12–15, 450–600 ka, the upwelling can be estimated as strong as in interglacial stage of the present cycles, with slightly weak upwelling in the glacial stage. This upwelling and climate can be traced back to the late Pliocene. The strongest upwelling can be estimated in the Pliocene-Pleistocene time by the isotopic indicators and the high organic carbon content.

INTRODUCTION

The primary object of ODP Leg 117, Neogene Package, was to clarify the monsoonal upwelling history in the northwestern Indian Ocean. To achieve this goal a series of sites was drilled along a depth transect in the Oman Margin, crossing through the oxygen minimum zone and thermocline (Prell, Niitsuma, et al., 1989; Figs. 1 and 2).

This paper presents the results of high resolution isotopic measurements on the sedimentary sequence of Site 723 located on the center of the oxygen minimum zone and the middle part of the thermocline, and discusses the paleoclimatology and history of the upwelling on the Oman Margin, related to the southwest monsoon in the northwestern Indian Ocean.

SITE

Site 723 is located in the center of the mid-slope basin of the Oman Margin. The subsiding sedimentary basin developed along the inner side of the sill which consists of tectonically growing en-echelon anticlines resulting from right lateral movement (Fig. 1).

SAMPLES

Above 85 mbsf, Hole 723A was drilled by advanced hydraulic piston corer (APC). However, below 40 mbsf, gas expansion developed after the core recovery. Below 85 mbsf, the extended core barrel (XCB) was used and gave poor recovery. Hole 723B was drilled by APC for upper 80 m, and then drilled by XCB. The apparent recovery was almost complete above 140 mbsf, however, gas expansion appeared from 40 mbsf and developed seriously below 80 mbsf.

The recovered sediments consist of marly nannofossil ooze intercalated by finely laminated siliceous-marly ooze and dolomitic calcareous concretions.

Shipboard sampling at 75 cm intervals was done by taking two samples routinely from each section all through the drilled sediments of Hole 723A (0–384.77 mbsf) and 723B (82.00–405.06 mbsf). Sample volume was 10 cm^3. Shore-based sampling at 20–25 cm intervals was done for 0–91.31 mbsf of Hole 723A and from 86.66 to 140.18 mbsf of Hole 723B. Furthermore, 20–25 cm interval samples from 17 to 82 mbsf of Hole 723B were taken to complete the missing stratigraphic intervals in Hole 723A, caused by the coring gaps and whole-round geochemical sampling gaps, based on precise layer-by-layer correlation (Niitsuma, this volume). The sampling gaps from gas expansions in Hole 723B at 100, 110, 120, and 130 mbsf could not be filled by Hole 723A sampling because of poor recovery and lack of lithologic markers.

The depth of the samples used in this paper is corrected for coring disturbance and gas expansion, based on layer-by-layer correlation and measurement on core photographs (Niitsuma,
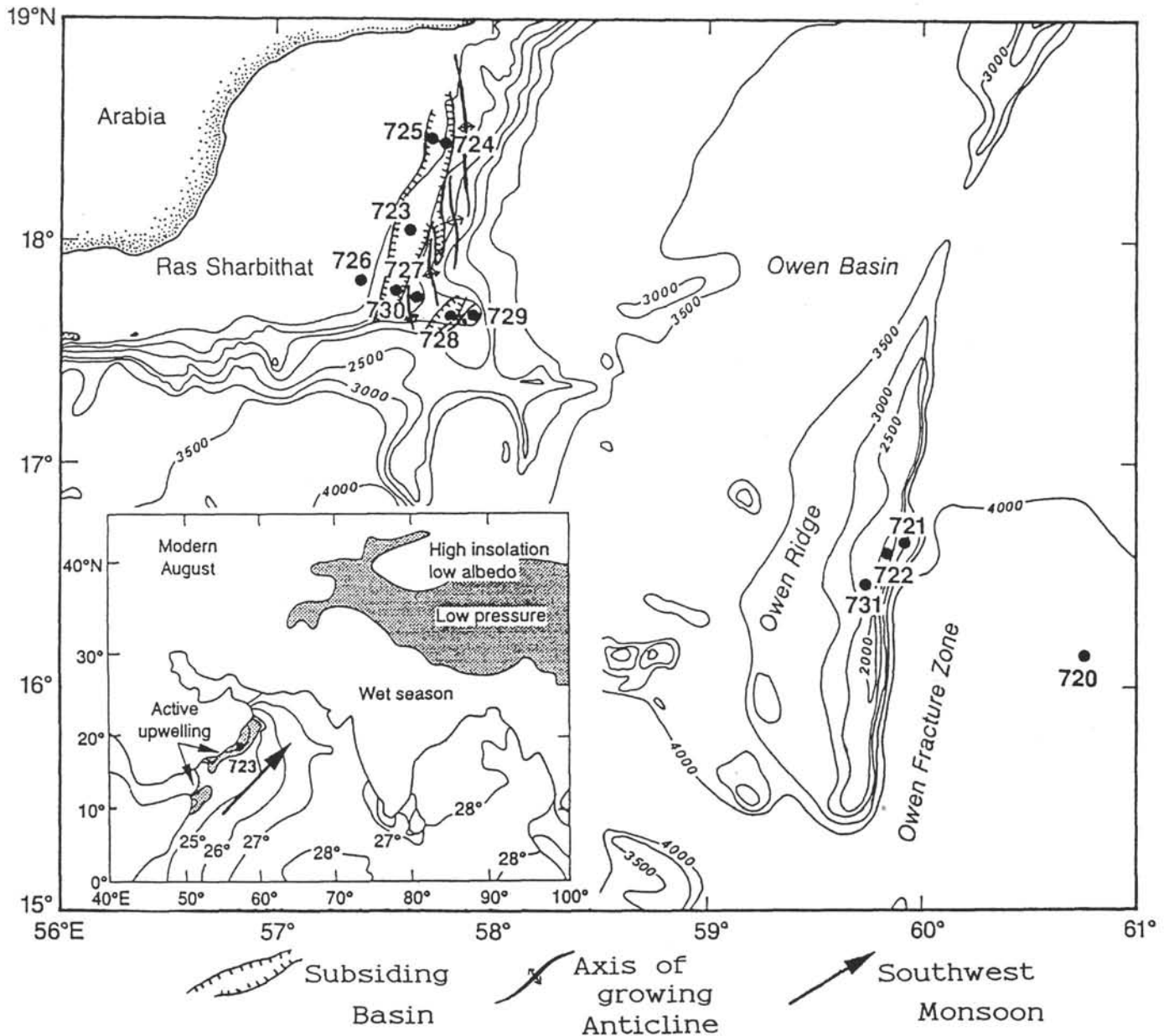
Figure 1. Location of Site 723 in the center of the subsiding basin in the Oman Margin and southwest monsoon (Prell, Niitsuma, et al., 1989).

this volume). Below 140 mbsf, ODP core log data were used for calculation of sample depth. In samples containing gas expansion voids, all the voids were closed and all separated sediment cores were pushed to the core top.

ANALYTICAL METHOD

The sediment sample was soaked in hot water for 12 hr and wet-sieved through 200 mesh (74 μm). The sieved sample was cleaned with ultrasonic wave and dried. Then the sample was dry-sieved through 64 mesh (230 μm).

The tests of the following foraminiferal species were used for the isotopic analysis: planktonic, *Pulleniatina obliquiloculata* (Parker and Jones); benthic, *Uvigerina excellens* Todd.

Ten or more tests of the species, picked up under a binocular microscope, were put in a stainless-steel thimble. Methyl alcohol was dropped into the thimble, the tests were disaggregated with a thin needle and cleaned with ultrasonic wave, and the methyl alcohol was sucked out with a syringe and then evaporated.

The isotopic measurement followed the procedure by Wada et al. (1984). The carbonate tests were reacted in saturated pyrophosphoric acid at 60.00°C, and the resulting CO_2 gas was analyzed with MAT-250 and MAT-251 mass spectrometers modified for ultra-small sample analysis. The value thus obtained was converted into a value against a PDB standard by using NBS 20. The converted values are $-4.18‰$ for $\delta^{18}O$ and $-1.07‰$ for $\delta^{13}C$ (Craig, 1957).

The precision for isotopic analyses is 0.02‰ for carbon and 0.05‰ for oxygen. Minimum volume for the isotopic analyses is 1 μL for MAT-250 of Shizuoka and 2 μL for MAT-251 of Kanazawa. The standard deviations of eight duplicated measurements on the isotopes for each individual test of foraminifer have ranges of 0.1‰–0.27‰ for planktonic carbon, 0.18‰–0.36‰ for planktonic oxygen, 0.09‰–0.19‰ for benthic carbon, and 0.07‰–0.28‰ for benthic oxygen.

The foraminiferal specimens for isotopic analysis can be picked up easily in the upper part of the sedimentary sequence, how-
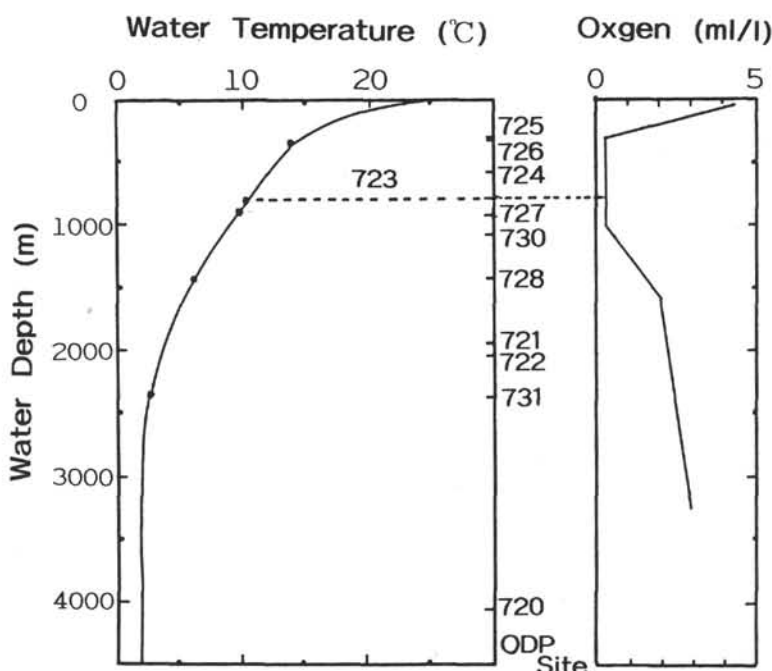
Figure 2. Depth profile of the measured temperature and dissolved oxygen (Prell, Niitsuma, et al., 1989) in the northwestern Indian Ocean, and ODP sites.

ever, specimens are less common in the lower part. Generally benthic foraminifers dominate in the dark colored sediment samples, and planktonic foraminifers in the white colored samples. Black samples in the lower part do not contain foraminiferal tests, but do contain fish teeth. The sample intervals in the lower part of the sequence are not close, compared with the upper part, because of the poor core recovery, gas expansion, and the nonpreservation of the foraminifers.

OXYGEN ISOTOPE STRATIGRAPHY

Oxygen isotope curve of planktonic $\delta^{18}O_P$ and benthic $\delta^{18}O_B$ from Site 723 (Figs. 3 and 4 and Table 1) can be correlated well with standard curves, for example, with Graphic Correlation Composite Records (Prell et al., 1986), SPECMAP (Imbrie et al., 1984), and Williams et al. (1988). Description and numerical coding of the oxygen isotope stratigraphic events in this paper follow Prell et al. (1986). Even numbered stages and substages represent glacial and/or colder intervals with heavier oxygen isotopic values, and odd numbered stages represent interglacial and/or warmer intervals.

Oxygen isotope curve of planktonic $\delta^{18}O_P$ can be traced back continuously to Stage 23 with high resolution measurements. A significant difference appeared in Stage 15.4 with comparably heavy values, and a peak of Stage 15.5 is separated from the main Stage 15 peak. The oxygen isotope stratigraphic correlation can not be defined clearly in the time interval older than Stage 23. A tentative correlation is made to Stage 53 and shown in Figure 3.

The benthic foraminiferal curve $\delta^{18}O_B$ can also be correlated with the standard oxygen isotope stratigraphic curve, however, the amplitude of the fluctuations of the curve is significantly small, especially older than Stage 16. The maximum differences of benthic oxygen isotope values relative to planktonic differences between glacial and interglacial stages are 92.5% for Stages 1–2, 76.1%–89.0% for Stages 5–16, 9.3% for Stages 17–18, and 38.4% for Stages 21–22.

Nannofossil biostratigraphic datums (Spaulding, this volume) can be located within the oxygen isotope stratigraphy (Figs. 3 and 4 and Table 1), last appearance of *Helicosphaera inversa* at

Stage 6.2, first appearance of *Emiliania huxleyi* at Stages 9.0–8.5, last appearance of *Pseudoemiliania lacunosa* at Stage 12.3, top acme of *Reticulofenestra* sp. A at Stages 23–25, first appearance of *Gephyrocapsa parallela* at Stages 27–29, last appearance of *Gephyrocapsa* (large) at Stages 34–35, and last appearance of *Helicosphaera sellii* at Stages 42–44.

FLUCTUATION OF OXYGEN ISOTOPE RATIO

The oxygen isotope values are controlled by oxygen isotopic composition and temperature of seawater. The contributions of the two factors can be quantified by comparing the oxygen isotope values of benthic and planktonic foraminifers. The difference of oxygen isotope $\delta^{18}O_{B-P}$ is 2.3‰ in the Holocene sample of Site 723, corresponding to a temperature difference of about 10°C. This is the same as the present temperature difference in the water column (Fig. 2), because the planktonic species *Pulleniatina* lives in the water depths from 25 to 74 m and precipitates its test under isotopic equilibrium (Kahn, 1979). In the case of Site 720 on the Indus Fan with water depth of 4045 m, the isotope differences $\delta^{18}O_{B-P}$ are 4‰ of which the corresponding temperature differences are 17°C, and consistent also with present water column (Yasuda et al., this volume). The consistencies suggest that the isotope differences $\delta^{18}O_{B-P}$ represent mainly temperature differences between the surface and bottom of the seawater in this area.

The oxygen isotope differences $\delta^{18}O_{B-P}$ of Site 723 have a wide range from 1.5‰ to 3.5‰. Because the amplitude of the fluctuations of the benthic curve $\delta^{18}O_B$ is significantly less than that of the planktonic foraminifer $\delta^{18}O_P$ as mentioned above, the larger differences appear in the lighter oxygen isotope stages, i.e., in the interglacial stages. The amplitude of $\delta^{18}O_{B-P}$ fluctuation for Stages 1–13 except the spikes is about 1‰, of which the equivalent temperature is 4°C. The corresponding salinity difference is quite larger (4‰), which is comparable to the influx of river water in the Bengal Bay (Duplessy, 1982).

The influence of the sea level change should count as a candidate for the explanation of the $\delta^{18}O_{B-P}$ fluctuation; however, the measured temperature gradient is 0.8°C/100 m for the depth
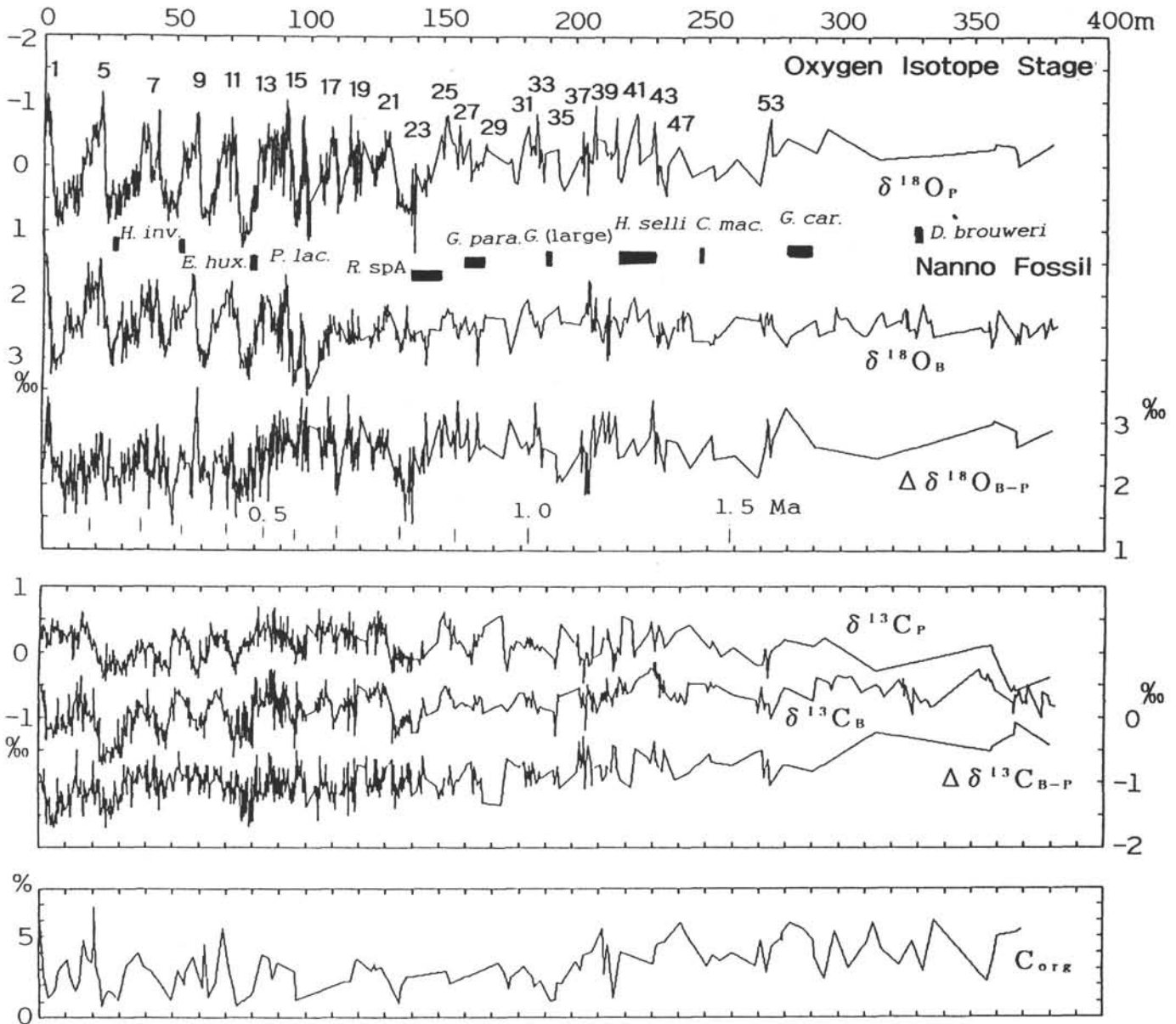
Figure 3. Isotopic results, organic carbon contents, and nannofossil biostratigraphic horizons of Site 723 in the Oman Margin. Number: oxygen isotope stratigraphic stages. $\delta^{18}O_P$ and $\delta^{13}C_P$: oxygen and carbon isotope of planktonic foraminifer *Pulleniatina obliquiloculata*. $\delta^{18}O_B$ and $\delta^{13}C_B$: oxygen and carbon isotope of benthic foraminifer *Uvigerina excellens*. $\delta^{18}O_{B-P}$ and $\delta^{13}C_{B-P}$: difference of oxygen and carbon isotope between benthic $\delta^{18}O_B$ and $\delta^{13}C_B$, and planktonic $\delta^{18}O_P$ and $\delta^{13}C_P$. C_{org}: organic carbon content.

range from 330 to 800 m (Fig. 2) and the contribution of 100 m sea level change for the oxygen isotope is only 0.2‰.

Site 723 is located in the central part of the monsoonal upwelling area and the present SST (sea surface temperature) in summer is significantly cooled by the upwelling, 23°–24°C which is almost same as the winter SST in this area (Prell and Hutson, 1979). The upwelling reduces the seasonal fluctuation of SST. SST for the Last Glacial Maximum, Stage 2, has been also estimated as almost the same as at present, because of cancelling the global cooling by the weakened monsoonal upwelling, based on isotopic and faunal data (Prell and Hutson, 1979). These data suggest that the oxygen isotope curve of planktonic $\delta^{18}O_P$ may represent rather the oxygen isotope fluctuation of seawater relating to the volume of global ice sheet, which is presented as the standard curves of oxygen isotope stratigraphy

than the SST fluctuation, and the $\delta^{18}O_{B-P}$ fluctuation should be mainly caused by the bottom water.

The $\delta^{18}O_{B-P}$ fluctuation suggests that the bottom temperature was warmer and/or the isotopic composition of bottom water was affected by fresh water influx in the glacial stage.

Because the 800 m depth of Site 723 is in the center of the thermocline, the bottom temperature is sensitive to the position of the thermocline. During the strong upwelling stage, the thermocline would be pushed up and the bottom temperature should be cool, which is consistent with the cooler temperature in the interglacial stages with stronger southwest monsoon than in glacial stages.

Significant delays of benthic oxygen isotopes $\delta^{18}O_B$ from the planktonic $\delta^{18}O_P$ appear in the transgressive stages, Stages 10–9, Stages 6–5, and Stages 2–1. The occurrence of the delay in the
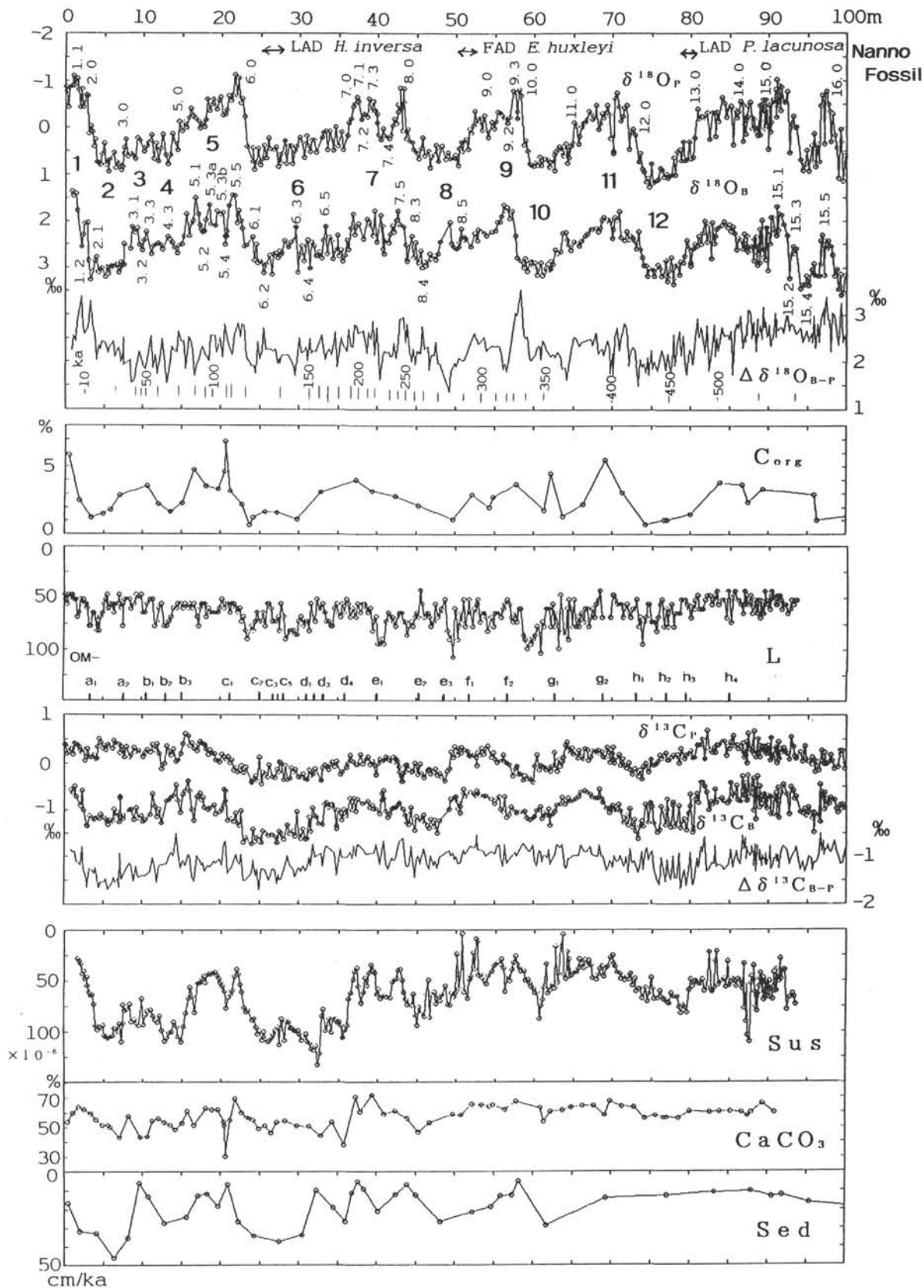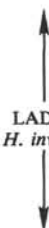
Figure 4. Isotopic results, nannofossil biostratigraphic horizons, and available data sets. Number: oxygen isotope stratigraphic stages. $\delta^{18}O_P$ and $\delta^{13}C_P$: oxygen and carbon isotope of planktonic foraminifer *Pulleniatina obliquiloculata*. $\delta^{18}O_B$ and $\delta^{13}C_B$: oxygen and carbon isotope of benthic foraminifer *Uvigerina excellens*. $\delta^{18}O_{B-P}$ and $\delta^{13}C_{B-P}$: difference of oxygen and carbon isotope between benthic $\delta^{18}O_B$ and $\delta^{13}C_B$, and planktonic $\delta^{18}O_P$ and $\delta^{13}C_P$. C_{org}: organic carbon content. L: lightness of sediment color (upside = dark). Sus: magnetic susceptibility. $CaCO_3$: calcium carbonate content. Sed: rate of sedimentation.

Table 1. Isotopic results of planktonic, *Pulleniatina obliquiloculata* ($\delta^{13}C_B$, $\delta^{18}O_P$) and benthic foraminifers, *Uvigerina excellens* ($\delta^{13}C_B$, $\delta^{18}O_P$) with remarks on the oxygen isotope stratigraphic horizon and nannofossil biostratigraphic horizon (Spaulding, this volume) at Site 723.

Hole, core, section, interval (cm)	Depth (mbsf)	$\delta^{13}C_P$	$\delta^{18}O_P$	$\delta^{13}C_B$	$\delta^{13}O_B$	$\delta^{18}O$ Stage	Nannofossil datum
			‰ PDB				
A-1H-1, 7	0.07	0.389	−0.877			1.0	
A-1H-1, 21	0.21	0.357	−0.777				
A-1H-1, 41	0.41	0.209	−0.451				
A-1H-1, 61	0.61	0.231	−0.858				
A-1H-1, 81	0.81	0.300	−0.892	−0.563	1.364		
A-1H-1, 101	1.01	0.295	−1.101	−0.618	1.455	1.1	
A-1H-1, 116	1.16	0.187	−0.902				
A-1H-1, 131	1.31	0.399	−1.011	−0.493	1.420		
A-1H-1, 148	1.48	0.384	−1.035	−0.708	1.780		
A-1H-2, 21	1.71	0.374	−0.814				
A-1H-2, 41	1.91	0.342	−0.448				
A-1H-2, 61	2.11	0.270	−0.825	−0.910	2.553	1.2	
A-1H-2, 81	2.31	0.216	−0.447	−0.588	2.292		
A-1H-2, 101	2.51	0.289	−0.527	−0.994	2.052		
A-1H-2, 116	2.66	0.059	−0.700			1.3	
A-1H-2, 131	2.81	0.130	−0.687	−1.330	2.041	2.0	
A-1H-2, 146	2.96	0.297	0.118	−1.340	2.840		
A-1H-3, 21	3.21	0.147	−0.029	−1.118	3.256		
A-1H-3, 41	3.41	0.113	0.086				
A-1H-3, 61	3.61	0.134	0.414	−1.164	3.070		
A-1H-3, 78	3.78	0.177	0.252	−1.193	2.857		
A-1H-3, 101	4.01	0.087	0.746	−1.159	2.779	2.1	
A-1H-3, 116	4.16	0.108	0.773				
A-1H-3, 129	4.29	0.349	0.736	−1.152	3.098		
A-1H-3, 148	4.48	0.504	0.802	−1.175	3.046		
A-1H-4, 21	4.71	0.434	0.569	−1.094	3.009		
A-1H-4, 41	4.91	0.311	0.344				
A-1H-4, 61	5.11	0.381	0.807	−1.161	3.202	2.2	
A-1H-4, 81	5.31	0.288	0.720	−1.189	3.002		
A-1H-4, 101	5.51	0.375	0.944	−1.240	3.137		
A-1H-4, 116	5.66	0.383	0.697	−1.323	2.994		
A-1H-4, 131	5.81			−1.202	3.029		
A-1H-4, 145	5.95			−1.211	2.968		
A-1H-5, 21	6.21	0.320	0.541	−1.234	2.972		
A-1H-5, 41	6.41	0.461	0.859	−0.976	2.960		
A-1H-5, 61	6.61	0.414	0.741	−1.137	2.942		
A-1H-5, 81	6.81	0.408	0.792	−1.047	3.104		
A-1H-5, 101	7.01	0.397	0.849	−1.250	3.018		
A-1H-5, 116	7.16	0.227	0.904	−0.712	2.893		
A-1H-5, 116	7.16			−0.737	2.958		
A-1H-5, 131	7.31	0.341	0.853	−1.145	2.917		
A-1H-5, 148	7.48	0.275	0.434	−1.184	2.940		
A-2H-1, 31	7.51	0.301	0.565	−1.116	2.496	3.0	
A-2H-1, 51	7.71	0.136	0.253				
A-2H-1, 81	8.01	0.339	0.624				
A-2H-1, 116	8.36	0.143	0.560	−0.994	2.599		
A-2H-1, 141	8.61	0.191	0.583	−0.974	2.133		
A-2H-2, 21	8.91	0.329	0.669	−1.196	2.256	3.1	
A-2H-2, 51	9.21	0.260	0.224	−0.952	2.154		
A-2H-2, 81	9.51	0.276	0.281	−1.167	2.506	3.2	
A-2H-2, 116	9.86			−1.124	2.626		
A-2H-2, 141	10.11	0.154	0.514	−1.245	2.415		
A-2H-3, 21	10.41	0.217	0.400	−1.196	2.238	3.3	
A-2H-3, 51	10.71	0.288	0.333				
A-2H-3, 81	11.01	0.236	0.171	−1.082	2.712	4.0	
A-2H-3, 116	11.36	0.389	0.673	−0.639	2.534		
A-2H-3, 141	11.61	0.277	0.353	−0.921	2.512		
A-2H-4, 21	11.91	0.404	0.729	−1.127	2.482		
A-2H-4, 53	12.23	0.203	0.452	−0.982	2.508		
A-2H-4, 81	12.51	−0.105	0.143	−0.269	2.617		
A-2H-4, 116	12.86	−0.012	0.594				
A-2H-4, 141	13.11	0.358	0.794	−0.798	2.346	4.3	
A-2H-5, 21	13.41	0.253	0.588	−0.765	2.400		
A-2H-5, 51	13.71	0.182	0.136	−0.725	2.458		
A-2H-5, 81	14.01	0.302	0.323	−0.695	2.573		
A-2H-5, 116	14.36	0.033	0.485	−0.469	2.694	4.4	
A-2H-5, 141	14.61	0.078	−0.127	−0.785	2.519	5.0	
A-2H-6, 21	14.91	0.215	0.072	−1.035	2.489		
A-2H-6, 53	15.23	0.409	−0.116	−0.665	2.326		
A-2H-6, 81	15.51	0.622	0.003	−0.584	1.862		
A-2H-6, 116	15.86	0.580	−0.210	−0.376	2.315		
A-2H-6, 141	16.11	0.374	−0.411	−0.590	2.066		
A-2H-7, 18	16.38	0.427	−0.270	−0.981	1.989		
A-2H-7, 51	16.71	0.314	−0.198	−1.210	1.503	5.1	

Table 1 (continued).

Hole, core, section, interval (cm)	Depth (mbsf)	$\delta^{13}C_P$	$\delta^{18}O_P$	$\delta^{13}C_B$	$\delta^{13}O_B$	$\delta^{18}O$ Stage	Nannofossil datum
			‰ PDB				
B-3H-3, 21	17.01	0.274	−0.137	−0.712	1.862		
B-3H-3, 41	17.21	0.397	0.019	−0.669	2.086		
B-3H-3, 63	17.43	0.452	−0.062	−0.633	2.168		
B-3H-3, 81	17.61	0.425	−0.083	−0.765	2.243	5.2	
B-3H-3, 101	17.81	0.401	−0.020	−0.725	2.226		
A-3H-1, 16	17.96	0.389	−0.167	−0.940	1.983		
A-3H-1, 41	18.21	0.300	−0.612				
A-3H-1, 66	18.46	0.190	−0.367	−0.988	1.651	5.3a	
A-3H-1, 91	18.71	0.281	−0.488	−0.951	2.070		
A-3H-1, 116	18.96	0.211	−0.611				
A-3H-1, 141	19.21	0.215	−0.462	−0.884	2.096		
A-3H-2, 16	19.46	0.067	−0.407	−1.073	1.800		
A-3H-2, 41	19.71	0.075	−0.584				
A-3H-2, 64	19.94	0.030	−0.655	−1.025	1.853	5.3b	
A-3H-2, 91	20.21	0.191	−0.272	−0.987	1.819		
A-3H-2, 116	20.46			−0.890	2.321		
A-3H-2, 116	20.46	0.153	−0.296	−0.550	2.496	5.4	
A-3H-2, 141	20.71	0.086	−0.378	−0.586	2.220		
A-3H-2, 141	20.71			−0.792	2.331		
A-3H-3, 16	20.96	0.140	−0.696	−1.206	1.670		
A-3H-3, 41	21.21	0.016	−0.585				
A-3H-3, 66	21.46	0.066	−0.704	−1.181	1.438	5.5	
A-3H-3, 91	21.71	−0.145	−1.139	−1.243	1.456		
A-3H-3, 116	21.96	−0.093	−0.689	−1.050	2.038		
A-3H-3, 141	22.21	−0.169	−1.056	−1.267	1.779		
A-3H-4, 16	22.46	−0.161	−0.534	−1.338	1.990		
A-3H-4, 41	22.71	−0.059	−0.636	−1.017	2.161		
A-3H-4, 64	22.94	−0.181	−0.249	−1.685	2.535	6.0	
A-3H-4, 91	23.21	−0.082	0.408	−1.588	2.510		
A-3H-4, 116	23.46						
A-3H-5, 16	23.96	−0.407	0.729				
A-3H-5, 16	23.96	−0.376	0.443	−1.722	2.349	6.1	
A-3H-5, 41	24.21	−0.328	0.900	−1.412	2.823		
A-3H-5, 65	24.45	−0.262	0.735	−1.671	2.499		
A-3H-5, 91	24.71	−0.352	0.458	−1.609	2.890		
A-3H-5, 116	24.96	0.137	0.806	−1.567	2.859		
A-3H-5, 141	25.21	−0.436	0.670	−1.696	2.912		
A-3H-6, 16	25.46	−0.183	0.393	−1.447	3.110	6.2	
A-3H-6, 41	25.71	−0.212	0.655	−1.499	2.926		LAD of
A-3H-6, 66	25.96	−0.281	0.221				H. inversa
A-3H-6, 91	26.21	−0.039	0.455	−1.541	2.740		
A-3H-6, 116	26.46			−1.522	3.132		
A-3H-6-141	26.71	−0.280	0.470	−1.537	2.705		
A-3H-7, 14	26.94	−0.299	0.419	−1.582	2.695		
A-3H-7, 41	27.21	−0.131	0.831	−1.702	2.790		
A-3H-7, 61	27.41	−0.177	0.582	−1.559	2.645		
B-4H-3, 43	27.53	0.023	0.764	−1.459	2.718		
B-4H-3, 65	27.75	0.003	0.564	−1.491	2.694		
A-4H-1, 16	28.06	−0.334	0.287	−1.627	2.426		
A-4H-1, 41	28.31	−0.059	0.778				
A-4H-1, 66	28.56	−0.334	0.399	−1.317	2.551		
A-4H-1, 91	28.81	−0.312	0.389	−1.493	2.448		
A-4H-1, 116	29.06	−0.095	0.770				
A-4H-1, 141	29.31	−0.178	0.494	−1.457	2.403		
A-4H-2, 16	29.56	−0.128	0.410	−1.556	2.131	6.3	
A-4H-2, 41	29.81			−1.027	3.085		
A-4H-2, 62	30.02	−0.273	0.215	−1.496	2.729		
A-4H-2, 91	30.31	−0.287	0.329	−1.603	2.520		
A-4H-2, 116	30.56	−0.225	0.630	−1.412	2.842		
A-4H-2, 141	30.81	−0.322	0.185	−1.625	2.509		
A-4H-3, 16	31.06	−0.346	0.391	−1.610	2.407		
A-4H-3, 41	31.31	−0.139	0.509	−1.156	3.004	6.4	
A-4H-3, 66	31.56	−0.257	0.264	−1.457	2.448		
A-4H-3, 91	31.81	−0.226	0.269	−0.956	2.523		
A-4H-3, 116	32.06	−0.114	0.531	−1.124	2.746		
A-4H-3, 141	32.31			−1.132	2.736		
A-4H-4, 16	32.56			−1.290	2.663		
A-4H-4, 41	32.81	−0.350	0.214	−1.274	2.781		
A-4H-4, 62	33.02	−0.102	0.098	−1.302	2.401		
A-4H-4, 91	33.31	−0.030	0.069	−0.870	2.116	6.5	
A-4H-4, 116	33.56	−0.068	0.470	−0.835	2.686		
A-4H-4, 141	33.81	−0.121	0.066	−0.937	2.349		
A-4H-5, 16	34.06	−0.025	0.267	−0.881	2.419		
A-4H-5, 41	34.31	0.021	0.481	−0.867	2.794		
A-4H-5, 66	34.56	−0.062	−0.013	−0.965	2.635		
A-4H-5, 91	34.81	0.040	0.399	−1.337	2.299		
A-4H-5, 91	34.81			−1.385	2.583		

Table 1 (continued).

Hole, core, section, interval (cm)	Depth (mbsf)	$\delta^{13}C_P$	$\delta^{18}O_P$	$\delta^{13}C_B$	$\delta^{13}O_B$	$\delta^{18}O$ Stage	Nannofossil datum
			‰ PDB				
A-4H-5, 116	35.06			− 1.003	2.733		
A-4H-5, 141	35.31	− 0.224	0.095	− 1.051	2.615		
A-4H-6, 16	35.56	−0.176	0.461	− 1.200	2.846	6.6	
A-4H-6, 41	35.81			− 0.981	2.729		
A-4H-6, 66	36.06	− 0.086	0.163	− 1.106	2.399		
A-4H-6, 91	36.31	0.006	− 0.108	− 0.993	2.595	7.0	
A-4H-6, 116	36.56	0.170	− 0.201	− 0.732	2.141		
A-4H-6, 141	36.81	0.062	− 0.463	− 0.974	1.858		
A-4H-7, 16	37.06	0.032	− 0.526	− 0.743	2.275		
A-4H-7, 41	37.31	− 0.019	− 0.654	− 1.013	2.108	7.1	
A-4H-7, 64	37.54	− 0.022	− 0.563	− 0.750	2.047		
A-5H-1, 31	37.91	0.199	− 0.190			7.2	
A-5H-1, 65	38.15	− 0.009	− 0.306	− 0.847	2.368		
A-5H-1, 91	38.39	0.065	− 0.288				
A-5H-1, 121	38.69	0.102	− 0.241	− 0.849	1.962		
A-5H-1, 141	38.89	0.145	− 0.636	− 0.800	2.008	7.3	
A-5H-2, 16	39.14	− 0.015	− 0.387	− 0.942	2.094		
A-5H-2, 41	39.39	0.048	− 0.567	− 0.885	2.302		
A-5H-2, 63	39.61	− 0.038	− 0.385	− 0.964	1.777		
A-5H-2, 91	39.89	− 0.233	− 0.314	− 0.969	2.428		
A-5H-2, 91	39.89	− 0.212	− 0.106				
A-5H-2, 116	40.14	− 0.004	0.147				
A-5H-2, 141	40.39	0.104	0.250	− 1.056	1.877		
A-5H-3, 16	40.64	0.053	0.004	− 0.774	2.099		
A-5H-3, 16	40.64			− 0.638	2.594		
A-5H-3, 41	40.89	0.070	0.163	− 0.574	2.413		
A-5H-3, 41	40.89			− 0.738	2.694		
A-5H-3, 66	41.14	0.142	0.188	− 1.004	2.387		
A-5H-3, 91	41.39	0.125	0.221	− 1.134	2.451	7.4	
A-5H-3, 116	41.64	0.067	0.146	− 1.075	2.265		
A-5H-3, 141	41.89	0.048	− 0.046	− 0.963	2.087		
A-5H-4, 16	42.14	0.145	− 0.200	− 0.932	2.223		
A-5H-4, 41	42.39	0.110	− 0.097	− 0.941	1.980		
A-5H-4, 63	42.61	0.073	− 0.347				
A-5H-4, 63	42.61	− 0.011	− 0.509	− 0.910	1.781	7.5	
A-5H-4, 91	42.89	− 0.174	− 0.853	− 0.835	2.070		
A-5H-4, 91	42.89	− 0.070	− 0.351				
A-5H-4, 116	43.12	− 0.370	0.052				
A-5H-4, 116	43.12	− 0.270	− 0.468				
A-5H-4, 139	43.33	− 0.197	− 0.546				
A-5H-4, 139	43.33	− 0.371	− 0.835	− 0.968	2.121	8.0	
A-5H-5, 16	43.60	− 0.174	0.231				
A-5H-5, 16	43.60	− 0.029	0.065	− 1.099	2.488		
A-5H-5, 41	43.85			− 1.042	2.797		
A-5H-5, 41	43.85	− 0.028	0.029	− 1.248	2.841		
A-5H-5, 66	44.09	− 0.107	0.288	− 1.308	2.535		
A-5H-5, 91	44.34	− 0.166	0.312	− 0.939	2.316	8.3	
A-5H-5, 116	44.59	− 0.159	0.469	− 1.224	2.770		
A-5H-5, 141	44.82	0.012	0.503	− 1.417	2.445		
A-5H-6, 19	45.08	− 0.051	0.546	− 1.116	2.791		
A-5H-6, 41	45.28	− 0.218	0.649	− 1.191	2.877		
A-5H-6, 66	45.51	0	0.441	− 1.161	2.636		
A-5H-6, 92	45.75	− 0.199	0.212	− 1.188	2.986	8.4	
A-5H-6, 116	45.98	− 0.274	0.586	− 1.089	2.864		
A-5H-6, 141	46.21			− 1.265	2.944		
A-5H-7, 16	46.46	− 0.131	0.506	− 1.337	2.840		
A-5H-7, 41	46.71	− 0.110	0.852	− 1.373	2.688		
A-5H-7, 59	46.89	− 0.199	0.621	− 1.173	2.785		
B-6H-2, 141	47.21	− 0.173	0.561	− 1.352	2.723		
B-6H-3, 16	47.46	− 0.115	0.380	− 1.194	2.809		
B-6H-3, 41	47.71	− 0.238	0.717	− 1.482	2.696		
B-6H-3, 68	47.98	− 0.207	0.468	− 1.208	2.436		
B-6H-3, 91	48.21	− 0.270	0.390				
B-6H-3, 141	48.71	− 0.363	0.668				
B-6H-4, 16	48.96	− 0.161	0.531				
B-6H-4, 41	49.21	− 0.093	0.644	− 0.960	2.026		
A-6H-1, 12	49.42	0.253	0.629	− 0.732	2.458		
A-6H-1, 41	49.69	0.127	0.649	− 0.778	2.541		
A-6H-1, 68	49.86	0.354	0.577	− 0.710	2.573		
A-6H-1, 91	50.08	0.282	0.677	− 0.686	2.581		
A-6H-1, 116	50.26	0.194	0.803				↑
A-6H-1, 141	50.41			− 0.954	2.447		
A-6H-1, 141	50.41	0.330	0.435	− 0.806	2.534		
A-6H-2, 16	50.64	0.223	0.294	− 0.898	2.347		
A-6H-2, 16	50.64			− 1.043	2.165	8.5	
A-6H-2, 29	50.77	0.342	0.494				
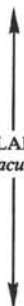
Table 1 (continued).

Hole, core, section, interval (cm)	Depth (mbsf)	$\delta^{13}C_P$	$\delta^{18}O_P$	$\delta^{13}C_B$	$\delta^{13}O_B$	$\delta^{18}O$ Stage	Nannofossil datum
				‰ PDB			
A-6H-2, 69	51.02	0.306	0.285	−0.537	2.328		FAD
A-6H-2, 69	51.02			−0.624	2.386		*E. huxleyi*
A-6H-2, 91	51.23	0.278	0.238	−0.670	2.355		
A-6H-2, 116	51.48	0.265	0.449				
A-6H-2, 142	51.71	0.172	0.026				
A-6H-3, 16	51.93	0.159	0.106	−0.607	2.542		
A-6H-3, 41	52.15	0.191	−0.050				
A-6H-3, 66	52.38	0.180	−0.374	−0.627	2.257		
A-6H-3, 91	52.56	0.135	−0.192	−0.662	2.308		
A-6H-3, 121	52.76	−0.038	−0.095	−0.574	2.399		
A-6H-3, 141	52.89	0.231	−0.218	−0.613	2.176		
A-6H-4, 16	53.13	0.189	−0.149				
A-6H-4, 16	53.13	0.190	−0.213	−0.656	2.213		
A-6H-4, 41	53.38	0.325	0.047				
A-6H-4, 63	53.58	0.201	−0.278	−0.678	2.258		
A-6H-4, 91	53.86	0.307	0.044	−0.682	2.292	9.0	
A-6H-4, 116	54.11	0.368	0.200				
A-6H-5, 16	54.61	0.150	−0.126	−0.735	2.226		
A-6H-5, 41	54.84	0.239	0.005				
A-6H-5, 66	55.08	0.104	−0.141	−0.837	2.197		
A-6H-5, 91	55.33	0.020	−0.355	−0.737	2.006	9.1	
A-6H-5, 118	55.60	0.052	−0.336	−0.697	2.004		
A-6H-5, 141	55.83	0.072	−0.298	−0.959	1.885		
A-6H-6, 16	56.08	0.192	−0.225	−1.006	1.635		
A-6H-6, 41	56.33	0.045	−0.220	−0.694	1.768		
A-6H-6, 66	56.58	0.008	−0.109	−1.138	1.697	9.2	
A-6H-6, 91	56.83	−0.016	−0.253	−1.073	1.931		
A-6H-6, 118	57.10			−0.922	1.781		
A-6H-6, 141	57.33	−0.251	−0.790				
A-6H-7, 16	57.58	−0.111	−0.760	−1.006	2.291		
A-6H-7, 41	57.82	−0.067	−0.362				
A-6H-7, 41	57.82	−0.059	−0.214	−1.048	2.773		
A-6H-7, 66	58.06	−0.217	−0.820			9.3	
A-6H-7, 87	58.25	−0.199	−0.706	−1.024	2.832	10.0	
B-7H-3, 66	58.64	−0.345	0.367	−1.041	2.960		
B-7H-3, 91	58.89	−0.252	0.268	−1.005	2.783		
B-7H-3, 116	59.14	−0.310	0.500	−1.147	3.054		
B-7H-3, 144	59.42	−0.298	0.773	−1.191	2.859		
B-7H-4, 16	59.64	−0.337	0.806	−1.172	2.847		
B-7H-4, 41	59.89	−0.384	0.813	−1.141	2.934		
B-7H-4, 61	60.09	−0.046	0.744	−1.123	2.869		
B-7H-4, 89	60.37	0.191	0.804	−0.995	3.128		
A-7H-1, 16	60.66	−0.120	0.618	−0.985	2.982		
A-7H-1, 35	60.85	−0.037	0.807	−0.924	2.875		
A-7H-2, 16	61.06	−0.051	0.687	−1.160	3.143		
A-7H-2, 38	61.28	−0.068	0.645	−1.045	3.071		
A-7H-2, 66	61.48	−0.122	0.707	−1.083	2.983		
A-7H-2, 91	61.70	−0.076	0.681	−1.105	2.908		
A-7H-2, 121	61.92	−0.115	0.840	−0.964	3.032		
A-7H-2, 141	62.12	−0.160	0.723	−1.320	2.843		
A-7H-2, 141	62.12			−1.110	3.016		
A-7H-3, 16	62.35	−0.030	0.715	−1.079	2.905		
A-7H-3, 47	62.53	−0.078	0.581				
A-7H-3, 47	62.53	0.231	0.905				
A-7H-3, 66	62.71	−0.043	0.507	−1.008	2.606		
A-7H-3, 91	62.94	−0.164	0.446	−0.890	2.678		
A-7H-3, 121	63.19	0.083	0.411				
A-7H-3, 142	63.37	−0.046	0.502	−0.862	2.645		
A-7H-4, 16	63.58	0.037	0.405	−0.702	2.258		
A-7H-4, 41	63.73	0.146	0.584				
A-7H-4, 66	63.97	0.385	0.349	−0.857	2.243		
A-7H-4, 91	64.15	0.454	0.751	−0.799	2.382		
A-7H-4, 127	64.39	0.350	0.415				
A-7H-4, 145	64.42	0.299	0.641	−0.727	2.489		
A-7H-5, 16	64.63	0.234	0.389	−0.802	2.621		
A-7H-5, 41	64.88	0.336	0.324				
A-7H-5, 68	65.09	0.209	−0.115	−0.760	2.429	11.0	
A-7H-5, 91	65.29	0.230	−0.039	−0.735	2.469		
A-7H-5, 126	65.59	0.110	0.343				
A-7H-5, 141	65.74	0.287	0.177	−0.686	2.522		
A-7H-6, 16	65.99	0.162	−0.013	−0.599	2.422		
A-7H-6, 41	66.24	0.103	−0.118				
A-7H-6, 66	66.49	0.320	−0.130	−0.571	2.312		
A-7H-6, 91	66.74	0.301	−0.206	−0.596	2.274		
A-7H-6, 116	66.97	0.072	−0.365				
A-7H-6, 141	67.22	0.146	−0.312	−0.642	2.180		

Table 1 (continued).

Hole, core, section, interval (cm)	Depth (mbsf)	$\delta^{13}C_P$	$\delta^{18}O_P$	$\delta^{13}C_B$	$\delta^{13}O_B$	$\delta^{18}O$ Stage	Nannofossil datum
			‰ PDB				
A-7H-7, 16	67.47	0.272	−0.181	−0.690	2.176		
A-7H-7, 41	67.70	0.240	−0.210				
A-7H-7, 66	67.95	0.269	−0.484	−0.721	2.141		
A-7H-7, 91	68.17	0.285	0.027	−0.717	2.214		
A-7H-7, 116	68.39	0.217	−0.095	−0.544	2.151		
A-7H-7, 141	68.62	0.259	−0.321	−0.736	1.971		
A-7H-8, 16	68.87	0.150	−0.229	−0.832	1.919		
A-7H-8, 41	69.12	0.133	−0.332				
A-7H-8, 66	69.37	0.341	−0.498	−0.958	1.958		
A-7H-8, 89	69.60	0.234	−0.300	−0.944	2.017		
B-8H-3, 31	69.75	0.031	0.219	−1.049	1.979		
B-8H-3, 66	69.96	0.208	0.156	−0.928	2.355		
B-8H-3, 83	70.13	0.050	0.498				
B-8H-3, 83	70.13	0.339	0.540	−0.885	2.170		
B-8H-3, 111	70.31	0.010	−0.637	−0.976	1.921		
B-8H-3, 139	70.59	0.123	−0.754	−0.981	1.983		
B-8H-4, 11	70.81	0.197	−0.464	−0.876	1.791		
A-8H-1, 16	71.06	−0.037	−0.150	−1.004	2.347		
A-8H-1, 41	71.31	0.108	−0.266				
A-8H-1, 66	71.56	−0.033	−0.433	−1.248	2.397		
A-8H-1, 91	71.81	−0.096	−0.495	−1.102	2.216		
A-8H-1, 116	72.06	0.013	0.447	−1.322	2.382		
A-8H-1, 141	72.31	−0.132	0.088	−0.973	2.319		
A-8H-2, 16	72.56	−0.225	0.020	−1.361	2.346		
A-8H-2, 41	72.81	−0.113	0.149	−1.189	2.421		
A-8H-2, 63	73.03			−1.451	2.580		
A-8H-2, 91	73.30	−0.269	0.726	−1.609	2.225		
A-8H-2, 116	73.54	−0.137	0.538	−1.347	2.603	12.0	
A-8H-2, 141	73.77	−0.331	0.874	−1.224	2.765		
A-8H-3, 15	74.01	−0.066	0.939	−1.340	2.930		
A-8H-3, 41	74.24	−0.007	1.157	−0.874	2.933		
A-8H-3, 66	74.47	−0.098	1.076	−0.916	3.171		
A-8H-3, 91	74.71	−0.172	1.265	−1.252	3.004		
A-8H-3, 116	74.94	0.081	0.780	−0.836	3.042		
A-8H-3, 141	75.14	−0.040	1.187	−0.923	3.033		
A-8H-4, 16	75.38	−0.036	1.146	−1.276	3.169		
A-8H-4, 41	75.63	−0.001	1.122				
A-8H-4, 62	75.84	0.047	1.091	−1.466	2.920		
A-8H-4, 91	76.13	0.179	0.859	−1.420	2.991		
A-8H-4, 113	76.33	0.104	0.902	−0.920	3.164		
A-8H-4, 141	76.56	0.181	1.055	−1.075	3.139		
A-8H-5, 16	76.81	0.220	0.987	−1.320	2.831		
A-8H-5, 41	77.06			−0.757	3.174		
A-8H-5, 41	77.06	0.075	1.070	−0.986	3.266		
A-8H-5, 65	77.27	0.076	1.037	−1.255	3.054		
A-8H-5, 91	77.53	0.135	1.004	−1.360	2.764		
A-8H-5, 116	77.78	0.175	0.632	−0.817	3.215		
A-8H-5, 116	77.78			−0.884	3.328		
A-8H-5, 141	78.03	0.125	1.006	−1.340	2.932		
A-8H-6, 16	78.28	0.194	0.509	−1.271	2.926		
A-8H-6, 41	78.53	0.013	0.476	−0.909	3.142		
A-8H-6, 66	78.78	0.310	0.700	−1.378	2.849		
A-8H-6, 91	79.03	0.192	0.304	−1.227	2.873		LAD *P. lacunosa*
A-8H-6, 116	79.28	0.094	0.703	−1.182	2.737		
A-8H-6, 141	79.53	0.193	0.660	−1.417	2.401		
A-8H-7, 16	79.78	0.205	0.297	−1.059	2.574		
A-8H-7, 41	80.03	0.266	0.658	−0.646	2.875		
A-8H-7, 41	80.03			−0.905	2.933		
A-8H-7, 66	80.28	0.122	0.628	−1.469	2.582		
A-8H-7, 85	80.47	0.138	0.216	−1.393	2.566		
B-9H-4, 92	80.57			−0.745	2.487	13.0	
B-9H-4, 116	80.81	0.394	−0.419	−0.638	2.513		
B-9H-4, 141	81.06	0.393	−0.209	−0.836	2.319		
B-9H-5, 16	81.31	0.403	−0.266	−0.392	2.487		
B-9H-5, 41	81.56	0.514	−0.268	−0.394	2.259		
B-9H-5, 66	81.81	0.106	−0.224	−0.476	1.992		
B-9H-5, 91	82.06	0.701	−0.339	−0.603	2.439		
A-9H-1, 16	82.36	0.294	0.243	−0.977	2.064		
A-9H-1, 54	82.64			−0.794	2.778		
A-9H-1, 66	82.76	0.232	−0.333	−0.876	2.020		
A-9H-1, 91	83.01	0.346	−0.332	−0.805	2.470		
A-9H-1, 106	83.16	0.237	0.186	−0.539	2.315		
A-9H-1, 141	83.38	0.395	−0.359	−0.823	2.165		
A-9H-2, 16	83.57	0.397	−0.134	−0.760	2.123		
A-9H-2, 63	84.04	0.457	−0.662	−0.726	2.089		
A-9H-2, 91	84.30	0.470	−0.539	−0.800	2.011		
A-9H-2, 116	84.55	0.180	−0.244				

Table 1 (continued).

Hole, core, section, interval (cm)	Depth (mbsf)	$\delta^{13}C_P$	$\delta^{18}O_P$	$\delta^{13}C_B$	$\delta^{13}O_B$	$\delta^{18}O$ Stage	Nannofossil datum
		‰ PDB					
A-9H-2, 141	84.75	0.356	− 0.450	− 0.846	2.131		
A-9H-3, 16	84.93	0.314	− 0.412	− 0.784	2.072		
A-9H-3, 40	85.17	0.447	− 0.477	− 0.404	2.199		
A-9H-3, 67	85.44	0.583	0.366	− 0.652	2.118		
A-9H-3, 91	85.65	0.371	− 0.397	− 0.689	2.251	14.0	
A-9H-3, 116	85.89	0.396	− 0.233	− 0.470	2.599		
A-9H-3, 141	86.14	0.318	− 0.361	− 0.764	2.365		
A-9H-4, 16	86.38	0.360	− 0.567	− 0.795	2.410		
A-9H-4, 40	86.62	0.427	− 0.487				
B-10X-1, 16	86.66	0.279	0.280	− 0.262	2.583		
A-9H-4, 67	86.82	0.128	− 0.283	− 0.680	2.265		
B-10X-1, 41	86.86	0.203	− 0.087	− 0.650	2.460		
A-9H-4, 95	87.08	0.172	0.137	− 0.413	2.567		
B-10X-1, 66	87.11	0.456	− 0.178	− 0.585	2.617		
A-9H-4, 116	87.27	0.003	− 0.266	− 0.786	2.308		
B-10X-1, 91	87.34	0.639	− 0.476	− 0.253	2.646		
B-10X-1, 116	87.59	0.299	− 0.555	− 0.685	2.545		
A-9H-5, 33	87.83	0.264	− 0.233	− 0.597	2.538		
B-10X-1, 141	87.84	0.347	0.012	− 0.430	2.519		
B-10X-2, 16	88.09	0.675	− 0.023	− 0.307	2.836		
A-9H-5, 66	88.10	0.214	− 0.201	− 0.990	2.373		
B-10X-2, 41	88.31	0.277	− 0.006	− 0.468	2.603		
A-9H-5, 91	88.35	0.128	0.068	− 1.174	2.322		
B-10X-2, 64	88.54	0.505	− 0.016	− 0.260	2.919		
A-9H-5, 116	88.60	0.198	0.157	− 0.662	2.687		
A-9H-5, 141	88.85	0.153	− 0.484	− 0.933	2.178		
B-10X-2, 105	88.89	0.381	0.152	− 0.472	2.878		
B-10X-2, 116	89.00	0.270	− 0.151	− 0.688	2.653		
A-9H-6, 16	89.10	0.353	− 0.514	− 0.846	1.981		
B-10X-3, 41	89.22	0.301	− 0.318	− 0.661	2.583		
A-9H-6, 40	89.34	0.306	− 0.609	− 0.754	2.573		
B-10X-3, 92	89.41	0.357	0.013	− 0.653	2.751		
A-9H-6, 66	89.60	0.271	− 0.620	− 0.898	2.134		
B-10X-3, 116	89.65	0.206	− 0.059	− 0.726	2.820		
A-9H-6, 91	89.83	0.217	− 0.412	− 0.952	2.126		
B-10X-4, 16	89.95	0.373	0.451	− 0.678	3.040	15.0	
A-9H-6, 116	90.08	0.312	− 0.504	− 0.740	2.291		
B-10X-4, 41	90.20	0.067	0.091	− 0.708	2.474		
B-10X-4, 62	90.24	0.540	− 0.127	− 0.687	2.232		
A-9H-6, 141	90.33	0.181	− 0.532	− 1.079	1.912		
A-9H-7, 16	90.58	0.104	− 0.611	− 1.073	1.915		
B-10X-4, 116	90.66	0.197	− 0.514	− 0.825	2.154		
A-9H-7, 41	90.83	0.338	− 0.824	− 0.705	2.220		
B-10X-5, 16	90.93	0.314	− 0.246	− 0.620	2.292		
B-10X-5, 41	91.03	0.271	− 0.632	− 0.738	2.295		
A-9H-7, 66	91.08	0.007	− 1.022	− 1.098	1.691	15.1	
B-10X-5, 66	91.28	0.447	− 0.487	− 0.510	2.185		
A-9H-7, 89	91.31	0.095	− 0.899	− 1.154	1.836		
B-10X-5, 101	91.48	0.321	− 0.383				
B-10X-5, 116	91.62	0.235	− 0.874	− 0.613	1.873		
B-10X-5, 141	91.87	0.327	− 0.569	− 0.448	2.069		
B-10X-6, 16	92.12	0.253	− 0.557				
B-10X-6, 41	92.37	0.210	− 0.788	− 0.653	2.291		
B-10X-6, 66	92.62	0.089	0.523	− 1.071	3.205	15.2	
B-10X-6, 91	92.87	0.561	− 0.095	− 0.488	2.716		
B-10X-6, 116	93.12	0.358	− 0.260	− 0.571	2.538		
B-10X-6, 141	93.37	0.161	− 0.002	− 0.739	2.692		
B-10X-7, 10	93.56	0.099	− 0.016	− 0.695	2.590		
B-11X-1, 16	94.06	0.245	0.689	− 1.030	3.423		
B-11X-1, 70	94.37	0.044	0.918	− 1.054	3.345		
B-11X-1, 101	94.68	0.353	0.794	− 0.962	3.351		
B-11X-1, 116	94.83	0.087	0.483	− 1.107	3.161		
B-11X-1, 141	95.05	0.046	0.734	− 1.047	3.270		
B-11X-2, 8	95.19	0.042	0.920	− 0.942	3.367		
B-11X-2, 41	95.49	− 0.024	0.389	− 1.060	3.026		
B-11X-2, 96	95.61	0.133	0.725	− 1.159	3.148		
B-11X-2, 118	95.81	0.069	0.139	− 1.037	3.122		
A-11X-1, 105	95.85			− 1.465	2.908		
A-11X-1, 116	95.96	− 0.176	0.460				
B-11X-2, 141	96.04	0.054	0.831	− 1.068	3.146		
B-11X-3, 41	96.27	− 0.070	0.355	− 1.130	3.168		
B-11X-3, 66	96.50	− 0.143	0.724	− 1.086	3.164		
B-11X-3, 84	96.67	0.056	− 0.472	− 0.449	2.425		
A-11X-2, 40	96.70			− 1.244	2.914		
B-11X-3, 122	96.83	0.276	− 0.704	− 0.598	2.298		
B-11X-3, 141	97.02	− 0.003	− 0.539	− 0.651	2.591		
A-11X-2, 89	97.19	− 0.023	0.354	− 0.980	3.152		

Table 1 (continued).

Hole, core, section, interval (cm)	Depth (mbsf)	$\delta^{13}C_P$	$\delta^{18}O_P$	$\delta^{13}C_B$	$\delta^{13}O_B$	$\delta^{18}O$ Stage	Nannofossil datum
		‰ PDB					
B-11X-4, 19	97.25	0.228	−0.704	−0.608	2.417		
B-11X-4, 41	97.44	−0.026	−0.782	−0.889	2.597		
B-11X-4, 64	97.66	0.014	−0.502	−0.733	2.419		
B-11X-4, 116	97.78	0.020	−0.376	−0.854	2.532		
B-11X-4, 139	98.01	0.184	0.308	−0.724	2.536		
B-11X-5, 39	98.21	0.057	−0.308	−0.761	2.730	16.0	
B-11X-5, 90	98.52	−0.119	0.170	−0.772	3.171		
B-11X-5, 116	98.78	−0.050	0.441	−0.960	3.031		
B-11X-5, 141	98.96	−0.078	1.081	−1.037	3.451		
B-11X-6, 16	99.21	0.264	0.035	−0.885	3.138		
B-11X-6, 54	99.29	0.193	0.323	−0.960	3.570		
B-11X-6, 81	99.56	0.273	1.137	−0.872	3.550		
B-11X-6, 116	99.81	−0.106	0.603	−0.935	3.166		
B-11X-6, 141	100.02	0.007	1.078	−1.035	3.292		
B-11X-7, 16	100.20	0.168	0.967	−0.970	3.481		
B-11X-7, 34	100.38	0.414	0.540	−0.965	3.486		
B-12X-1, 16	103.56	0.234	0.254	−0.892	3.134		
B-12X-1, 41	103.73	0.312	−0.188	−0.737	2.726		
B-12X-1, 66	103.93	0.442	0.155	−0.771	2.911		
B-12X-1, 91	104.17	0.413	0.151	−0.806	3.060		
B-12X-1, 116	104.34	0.175	−0.032	−0.876	2.885		
B-12X-1, 141	104.59	0.660	0.535	−0.925	3.043		
B-12X-2, 16	104.81	0.646	0.505	−0.671	2.952		
B-12X-2, 41	105.01	0.340	0.130	−0.737	2.723		
B-12X-2, 63	105.23	0.421	0.434	−0.837	2.788		
B-12X-2, 89	105.49	0.350	0.596	−0.897	3.007		
B-12X-3, 16	105.70	−0.020	0.335	−0.604	2.578	17.0	
B-12X-3, 41	105.95	0.313	−0.210	−0.687	2.719		
B-12X-3, 66	106.20	0.487	0.276	−0.554	2.763		
B-12X-3, 91	106.45	0.333	0.078	−0.599	2.545		
B-12X-3, 116	106.70	0.289	0.216	−0.827	2.840		
B-12X-3, 141	106.95	0.256	0.178	−0.799	2.821		
B-12X-4, 16	107.18	0.255	0.036	−0.761	2.473		
B-12X-4, 41	107.43	0.385	−0.426	−0.584	2.959		
B-12X-4, 64	107.66	0.292	−0.333	−0.418	2.323		
B-12X-4, 91	107.93	0.346	−0.315	−0.693	2.361		
B-12X-4, 116	108.18	0.455	−0.611	−0.617	2.431		
B-12X-4, 141	108.43	0.305	−0.484	−0.688	2.617		
B-12X-5, 16	108.68	0.410	−0.150	−0.758	2.494		
B-12X-5, 41	108.93			−0.716	2.470		
B-12X-5, 66	109.18	0.553	−0.170	−0.759	2.486		
B-12X-5, 91	109.43	0.450	−0.436	−0.702	2.350		
B-12X-5, 109	109.61	0.322	−0.434	−0.879	2.513		
B-12X-6, 16	109.88	0.394	0.059	−0.734	2.523		
B-12X-6, 41	110.13	0.162	−0.116	−0.815	2.613	18.0	
B-12X-6, 66	110.38	0.147	0.716	−1.168	2.641		
B-12X-6, 91	110.63	0.213	−0.032	−1.014	2.638		
B-12X-6, 116	110.88	0.192	0.306	−1.032	2.635		
B-12X-6, 141	111.13	0.414	0.577	−1.006	2.436		
B-12X-7, 16	111.36	−0.015	0.481	−1.068	2.465		
B-12X-7, 41	111.61	0.067	0.528	−0.955	2.739		
B-12X-7, 51	111.71	0.142	0.542	−1.029	2.466		
B-13X-1, 16	113.08	0.400	0.088	−0.788	2.626		
B-13X-1, 45	113.37	0.298	0.045	−0.828	2.671		
B-13X-1, 66	113.57	0.430	0.116	−0.786	2.667		
B-13X-1, 116	113.81	0.294	0	−0.849	2.737		
B-13X-1, 141	114.06	0.325	0.035	−0.812	2.751		
B-13X-2, 11	114.26	0.376	−0.027	−0.818	2.687		
B-13X-2, 41	114.41	0.266	−0.184	−0.867	2.703		
A-13X-1, 41	114.51	0.080	−0.161	−0.691	2.764		
B-13X-2, 90	114.60	0.326	−0.159	−0.910	2.404		
B-13X-2, 116	114.86	0.229	−0.795	−0.850	2.625		
B-13X-2, 141	115.11	0.347	−0.032	−0.734	2.778		
B-13X-3, 5	115.23	0.385	−0.005	−0.732	2.659		
A-13X-1, 116	115.26	0.320	−0.256	−0.746	2.774		
B-13X-3, 41	115.44	0.232	−0.427	−0.851	2.706		
B-13X-3, 66	115.65	0.147	−0.068	−0.782	2.561		
B-13X-3, 116	115.93	0.038	0.013	−0.793	2.766		
A-13X-2, 41	116.01	0.133	−0.043	−0.543	2.524		
B-13X-3, 141	116.11	0.482	0.244	−0.707	2.712		
A-13X-2, 126	116.36	0.311	−0.261	−1.195	2.233		
B-13X-4, 16	116.36	0.622	0.291	−0.697	2.625		
B-13X-4, 43	116.50	0.153	−0.288	−0.811	2.646		
B-13X-4, 63	116.68	0.340	−0.058	−0.712	2.719		
B-13X-4, 116	116.94	0.313	0.526	−0.802	2.762		
A-13X-3, 41	117.01	0.281	−0.342				
B-13X-4, 141	117.18	0.334	0.159	−0.812	2.592		

Table 1 (continued).

Hole, core, section, interval (cm)	Depth (mbsf)	$\delta^{13}C_P$	$\delta^{18}O_P$	$\delta^{13}C_B$	$\delta^{13}O_B$	$\delta^{18}O$ Stage	Nannofossil datum
			‰ PDB				
B-13X-5, 16	117.41	0.240	0.015	−0.652	2.661		
B-13X-5, 43	117.65	0.465	0.406	−0.841	2.698		
A-13X-3, 116	117.76	0.238	−0.558				
B-13X-5, 66	117.88	0.044	−0.048	−0.876	2.648		
B-13X-5, 116	118.08			−0.880	2.723		
B-13X-5, 141	118.31	0.249	−0.051	−1.123	2.603		
B-13X-6, 16	118.43	0.173	0.240	−1.268	2.663		
A-13X-4, 61	118.46	0.221	−0.412	−0.397	2.348		
B-13X-6, 43	118.68	0.265	−0.006	−1.117	2.666		
B-13X-6, 57	118.82	0	0.435	−1.140	2.679	19.0	
A-13X-5, 41	119.69	0.215	−0.378	−0.494	2.731		
B-14X-1, 11	122.69	0.184	−0.016	−0.583	2.654		
B-14X-1, 66	122.97	−0.024	0.095	−0.621	2.835		
B-14X-1, 91	123.22	0.284	−0.180	−0.664	2.670	20.0	
B-14X-1, 116	123.46	0.412	0.036	−0.727	2.779		
B-14X-1, 141	123.71	0.471	0.196	−0.738	2.725		
B-14X-2, 11	123.88	0.466	0.292	−0.750	2.653		
B-14X-2, 71	124.15	0.416	0.031	−0.533	2.656		
B-14X-2, 91	124.35	0.419	0.292	−0.652	2.675		
B-14X-2, 116	124.57	0.255	0.303	−0.698	2.554		
A-14X-1, 147	124.72	0.304	−0.181	−0.604	2.453		
B-14X-3, 11	124.81	0.451	0.194	−0.696	2.551		
B-14X-3, 41	125.09	0.424	0.183	−0.685	2.564		
B-14X-3, 69	125.37	0.486	−0.177	−0.586	2.520		
B-14X-3, 91	125.59	0.491	0.048	−0.650	2.602		
B-14X-3, 116	125.84	0.550	−0.060	−0.531	2.676		
A-14X-2, 129	125.94	−0.034	−0.240	−0.663	2.333		
B-14X-3, 139	126.07	0.414	0	−0.581	2.720		
B-14X-4, 11	126.17	0.432	−0.153	−0.633	2.634		
B-14X-4, 64	126.45	0.250	−0.114	−0.575	2.550		
B-14X-4, 91	126.72	0.638	−0.039	−0.488	2.565		
A-14X-3, 116	126.94	0.144	−0.297	−0.487	2.596		
B-14X-4, 116	126.95	0.588	−0.240	−0.471	2.607		
B-14X-4, 141	127.20	0.457	0.007	−0.453	2.513	21.0	
B-14X-5, 11	127.40	0.301	−0.196	−0.494	2.492		
B-14X-5, 31	127.60	0.465	−0.225	−0.594	2.540		
B-14X-5, 71	127.95	0.571	−0.101	−0.665	2.556		
A-14X-4, 109	128.07	0.256	−0.331	−0.667	2.267		
B-14X-5, 91	128.14	0.340	−0.550	−0.654	2.362		
B-14X-5, 116	128.34	0.287	−0.240	−0.806	2.178		
B-14X-5, 141	128.59	0.457	−0.425	−0.659	2.235		
B-14X-6, 11	128.79	0.415	−0.394	−0.585	2.238		
B-14X-6, 41	129.09	0.291	−0.338	−0.466	2.428		
B-14X-6, 66	129.32	0.282	−0.287	−0.558	2.271		
B-14X-6, 91	129.57	0.377	−0.495	−0.617	2.161		
B-14X-6, 116	129.82	0.136	−0.536	−0.640	2.357		
B-14X-6, 141	130.07	0.430	−0.310	−0.508	2.320		
B-15X-7, 11	130.27	0.195	−0.289	−0.575	2.272	22.0	
B-15X-1, 16	132.46	−0.299	0.303	−0.939	2.523		
B-15X-1, 41	132.71	−0.204	0.638	−1.397	2.715		
B-15X-1, 64	132.94	0.126	0.318	−0.933	2.629		
B-15X-1, 88	133.18	−0.049	0.378	−1.170	2.691		
B-15X-1, 116	133.46	−0.285	0.587	−1.001	2.570		
B-15X-1, 141	133.71	0.078	0.591	−1.315	2.734		
B-15X-2, 16	133.96	−0.080	0.625	−1.103	2.747		
B-15X-2, 38	134.18			−1.264	2.885		
B-15X-2, 69	134.49	−0.120	0.405	−1.230	2.897		
B-15X-2, 91	134.71	−0.086	0.596	−1.234	2.769		
B-15X-2, 138	134.88	0.082	0.622	−1.113	2.740		
B-15X-3, 8	135.05	−0.015	0.629	−1.254	2.854		
B-15X-3, 38	135.25	−0.159	0.662	−1.265	2.735		
B-15X-3, 63	135.50	−0.139	0.701	−1.047	2.619		
B-15X-3, 116	135.73	0.042	0.613	−1.015	2.524		
B-15X-3, 141	135.98	0.002	0.555	−1.060	2.663		
A-15X-3, 146	136.20	−0.005	0.582	−1.145	2.694		
B-15X-4, 16	136.21	−0.031	0.679	−0.973	2.559		
B-15X-4, 43	136.39	−0.211	0.652	−0.961	2.560		
B-15X-4, 69	136.65	−0.003	0.714	−1.035	2.178		
B-15X-4, 96	136.77	−0.025	0.614	−1.032	2.333		
B-15X-4, 116	136.97	−0.022	0.677	−0.973	2.529		
B-15X-4, 141	137.20	−0.022	0.725	−1.121	2.481		
B-15X-5, 16	137.45	−0.093	0.607	−1.014	2.603		
B-15X-5, 45	137.73	−0.039	0.687	−0.936	2.652		
B-15X-5, 69	137.97	−0.073	0.495	−1.006	2.706		
A-15X-5, 119	138.16	−0.111	0.027	−0.955	2.620		
B-15X-5, 91	138.19	−0.127	0.621	−1.066	2.738		
B-15X-5, 116	138.42	−0.299	0.908	−1.001	2.625		

Table 1 (continued).

Hole, core, section, interval (cm)	Depth (mbsf)	$\delta^{13}C_P$	$\delta^{18}O_P$	$\delta^{13}C_B$	$\delta^{13}O_B$	$\delta^{18}O$ Stage	Nannofossil datum
		‰ PDB					
B-15X-5, 141	138.67	−0.054	0.571	−1.049	2.672		
B-15X-6, 16	138.92	−0.190	0.507	−1.092	2.716		
B-15X-6, 42	139.17	−0.182	0.553	−0.870	2.696		
A-15X-6, 117	139.30	−0.013	−0.044	−1.049	2.569		
B-15X-6, 67	139.42	−0.273	1.336	−1.059	2.744	23.0	
B-15X-6, 92	139.67	−0.232	0.142	−1.033	2.736		
B-15X-6, 116	139.91	0.001	0.117	−1.218	2.634		
B-15X-6, 141	140.16	−0.109	0.116				
B-16X-1, 15	142.05	−0.100	0.385	−1.229	2.569		
B-16X-1, 145	143.00	−0.181	0.177	−0.998	2.742		
B-16X-2, 15	143.20			−0.875	2.739		TOP Acm. *R.*sp. A
B-16X-2, 116	143.58	0.183	0.450	−0.990	2.653		
B-16X-3, 15	144.02	−0.098	−0.041	−0.686	3.109		
B-16X-3, 116	145.01	−0.020	0.234	−0.968	2.544	24	
B-17X-1, 41	149.31	0.167	−0.488	−0.892	2.549		
B-17X-1, 116	150.06	0.464	−0.122	−0.804	2.324		
B-17X-2, 51	150.86	0.521	−0.762	−0.594	2.376		
B-17X-2, 133	151.65	0.619	−0.793	−0.590	2.292	25	
B-17X-3, 67	152.17	0.422	−0.610	−0.509	2.225		
B-17X-3, 113	152.61			−0.509	2.311		
B-17X-4, 41	153.37	0.344	−0.340	−0.649	2.282		
A-17X-1, 102	153.77	0.505	−0.376	−0.538	2.286		
B-17X-4, 119	154.15	0.039	−0.350	−0.704	2.520		
B-17X-5, 41	154.78	0.206	−0.274	−0.670	2.465		
A-17X-2, 110	155.25	0.412	0.032	−0.717	2.468	26	
B-17X-5, 116	155.46	0.355	−0.078	−0.826	2.626		
B-17X-6, 41	156.21	0.161	−0.641	−0.852	2.700	27	
B-17X-6, 116	156.96	0.138	−0.222	−0.802	2.441		
B-17X-CC, 41	157.39	0.193	−0.052	−0.794	2.535		
B-18X-1, 41	159.01	0.109	−0.311	−0.750	2.349		
B-18X-1, 121	159.81	0.011	−0.431	−0.814	2.627		
B-18X-2, 53	160.53	−0.059	0.213	−0.781	2.595	28	
B-18X-2, 121	161.01	−0.073	0.041				
B-18X-3, 41	161.71	0.040	0.055				LAD *G. parallela*
B-18X-3, 124	162.38	−0.174	−0.094	−0.844	2.424		
B-18X-4, 41	163.01	0.283	0.048	−0.891	2.724		
B-18X-4, 125	163.48	0.111	−0.063	−0.644	3.105		
B-18X-5, 54	164.01	0.104	−0.086	−0.798	2.519		
B-18X-5, 121	164.66	0.284	−0.016	−0.768	2.552		
B-18X-6, 41	165.24			−0.661	2.584		
B-18X-6, 121	166.04	0.235	−0.352	−0.696	2.310	29	
B-18X-7, 24	166.57	0.384	−0.263	−0.937	2.356		
A-19X-1, 116	173.26	0.567	−0.060	−0.788	2.370		
A-19X-2, 116	174.42	−0.071	−0.049				
A-19X-3, 116	175.61	−0.286	−0.120	−0.901	2.922		
A-19X-4, 104	176.70	0.118	0.221				
A-19X-5, 112	117.75	0.031	0.256			30	
A-19X-6, 116	178.76	0.177	−0.029				
A-19X-7, 116	180.25	0.159	−0.370	−0.612	2.211		
A-20X-1, 36	182.16	0.055	−0.638	−0.619	2.076	31	
A-20X-1, 132	182.79	0.239	−0.180	−0.822	2.310		
A-20X-2, 51	183.23	0.134	−0.326	−0.681	2.245		
A-20X-2, 139	183.81	0.245	−0.341	−0.717	2.329		
A-20X-3, 36	183.96	0.063	−0.240	−0.659	2.366		
A-20X-3, 138	184.74	0.203	−0.181	−0.844	2.490	32	
A-20X-4, 36	185.12	0.097	−0.806	−0.579	2.506	33	
A-20X-4, 145	185.74	0.054	−0.379	−0.761	2.401		
A-20X-5, 36	186.03	0.047	0.018				
A-20X-5, 133	186.66	0.138	−0.274	−0.875	2.664		
A-20X-6, 46	187.08	0.065	−0.166	−0.941	2.683		
A-20X-6, 127	187.69	0.023	0.22	−0.813	2.513	34	
A-20X-7, 36	188.08	0.106	−0.213	−0.840	2.389		LAD *G.* (large)
A-21X-2, 139	193.06	−0.097	−0.280	−0.906	2.207	35	
A-21X-3, 114	193.70	−0.233	0.127	−1.263	2.175		
A-21X-4, 103	194.54	0.142	0.279	−0.623	2.467		
A-21X-5, 134	195.55	0.429	0.361	−0.666	2.424	36	
A-22X-1, 41	201.51	0.103	−0.188				
A-22X-1, 118	201.98	0.280	−0.058	−0.550	2.461	37	
A-22X-2, 32	202.55	−0.162	−0.557	−0.523	2.335		
A-22X-2, 116	202.77	−0.192	0.136	−0.595	2.352		
A-22X-3, 32	203.36	−0.066	−0.305	−0.838	2.344		
A-22X-3, 144	204.00	−0.127	−0.393	−0.601	2.118		
A-22X-4, 41	204.36	−0.461	0.418	−0.740	2.287	38	
A-22X-4, 137	204.88	0.012	−0.225	−0.896	2.311		
A-22X-5, 41	205.14	−0.079	−0.134	−1.175	1.767		
A-22X-5, 141	205.84	0.003	−0.067	−0.482	1.813		
A-22X-6, 26	206.19	−0.198	−0.065	−0.625	2.593		

Table 1 (continued).

Hole, core, section, interval (cm)	Depth (mbsf)	$\delta^{13}C_P$	$\delta^{18}O_P$	$\delta^{13}C_B$	$\delta^{13}O_B$	$\delta^{18}O$ Stage	Nannofossil datum
			‰ PDB				
A-22X-6, 116	206.84			−0.565	2.536		
B-23X-1, 41	207.31	−0.154	−0.949	−0.873	2.177		
A-22X-7, 40	207.55	0.405	−0.132	−0.642	2.561		
B-23X-2, 41	207.73	−0.089	−0.429	−0.899	2.027	39	
A-22X-CC, 40	207.98			−0.598	2.339		
B-23X-3, 41	209.22			−0.925	2.500		
B-23X-3, 124	210.03			−0.832	2.731		
B-23X-4, 41	210.60	−0.021	−0.420	−0.726	2.759		
B-23X-4, 119	211.31	0.244	−0.187	−0.741	2.506		
A-23X-2, 56	211.96			−0.600	2.945		
A-23X-2, 26	212.31			−0.588	3.020		
A-23X-3, 32	213.13	0.185	−0.246	−0.691	2.927		
B-23X-6, 41	213.14	0.359	−0.131	−0.380	2.538		
B-23X-6, 93	213.66			−0.640	2.409		
B-23X-7, 36	214.34	0.06	−0.263				
B-24X-1, 139	217.74	−0.035	0.045			40	
B-24X-2, 105	218.90			−0.629	2.342		
B-24X-3, 39	219.37			−0.557	2.436		
B-24X-3, 101	219.84			−0.455	2.365		
B-24X-4, 41	220.54			−0.625	2.183		
A-24X-1, 41	220.81			−0.600	2.466		
A-24X-1, 116	221.56			−0.709	2.299		
B-24X-5, 35	221.95	0.476	−0.735	−0.601	2.018		
A-24X-2, 61	220.08			−0.712	2.104		
A-24X-2, 116	222.63			−0.746	2.015		
B-24X-6, 35	222.68	−0.028	−0.831				
B-24X-6, 125	223.08	−0.073	−0.700			41	
B-24X-7, 36	223.65	0.023	−0.048	−0.448	2.426		
A-24X-3, 127	223.95			−0.678	2.325		LAD
A-24X-4, 35	224.45	0.030	−0.548	−0.817	2.408		H. sellii
A-24X-4, 93	224.73	−0.284	−0.757	−0.705	2.363		
A-24X-5, 41	225.33	0.002	0.158				
A-24X-5, 113	226.05	−0.081	0.155	−0.540	2.588		
A-24X-6, 43	226.51	0.091	0.216	−0.683	2.673		
A-24X-6, 116	227.24			−0.370	2.553		
B-25X-1, 146	227.26			−0.316	2.227	42	
A-24X-7, 33	227.83	0.557	−0.115	−0.407	2.351		
B-25X-2, 140	228.24	0.282	−0.239	−0.317	2.529		
A-24X-CC, 41	228.28			−0.524	2.377		
B-25X-3, 116	229.38	0.474	−0.700	−0.222	2.661	43	
A-25X-1, 74	230.39	0.144	0.264	−0.284	2.617	44	
B-25X-4, 118	230.57			−0.139	2.685		
A-25X-2, 73	230.83	0.028	−0.048	−0.330	2.813		
A-25X-2, 111	231.19	0.305	−0.030	−0.350	2.741	45	
B-25X-5, 114	231.38			−0.143	2.416		
A-25X-3, 9	231.51	0.240	−0.026	−0.395	2.746		
A-25X-4, 68	232.02	0.415	0.148	−0.308	2.685		
A-25X-4, 111	232.25			−0.306	2.585		
B-25X-6, 106	232.30			−0.518	2.415		
A-25X-5, 68	232.68			−0.313	2.634		
B-25X-7, 22	232.76			−0.675	2.554		
A-25X-5, 111	232.84			−0.325	2.459		
A-25X-6, 55	233.78	0.208	0.437	−0.616	2.674	46	
A-25X-6, 110	234.25	0.071	−0.037	−0.415	2.677		
A-25X-7, 20	234.80			−0.601	2.832		
B-26X-1, 129	236.99			−0.720	2.485		
B-26X-2, 112	238.32			−0.598	2.566		
B-26X-3, 44	238.63	0.308	−0.329	−0.648	2.369	47	
B-26X-3, 120	239.39			−0.752	2.373		
B-26X-4, 31	239.87			−0.729	2.300		
A-26X-1, 40	240.20			−0.617	2.563		
B-26X-4, 111	240.39			−0.694	2.253		
A-26X-2, 33	240.94			−0.631	2.426		
A-26X-3, 30	241.66			−0.711	2.333		
A-26X-3, 90	242.01			−0.775	2.263		
A-26X-4, 33	242.79			−0.727	2.306		
A-26X-4, 115	243.53	0.419	0.147	−0.439	2.427		
A-26X-5, 3	243.71			−0.475	2.731		LAD
A-27X-1, 40	249.80			−0.475	2.731		C. macintyrei
A-27X-2, 40	250.70			−0.603	2.792		
A-27X-2, 125	251.38	0.512	−0.035	−0.510	2.761		
A-27X-3, 40	251.88			−0.449	2.767		
A-27X-3, 129	252.29	0.167	0.194	−0.514	2.613		
A-27X-4, 40	252.90			−0.535	2.684		
A-27X-4, 120	253.55			−0.487	2.663		
A-27X-6, 40	255.43	−0.068	0.085				
A-28X-1, 115	260.17	0.067	−0.128	−0.648	2.354		

Table 1 (continued).

Hole, core, section, interval (cm)	Depth (mbsf)	$\delta^{13}C_P$	$\delta^{18}O_P$	$\delta^{13}C_B$	$\delta^{13}O_B$	$\delta^{18}O$ Stage	Nannofossil datum
				‰ PDB			
A-29X-1, 40	269.10	−0.194	0.271	−0.724	2.404		
A-29X-1, 113	269.51			−0.924	2.277		
A-29X-2, 40	269.98			−0.697	2.491		
A-29X-3, 40	270.77			−0.521	2.632		
A-29X-3, 115	271.24	−0.189	−0.229	−0.688	2.328		
A-29X-4, 40	271.91	0.064	−0.485	−0.866	2.272		
A-29X-4, 108	272.38	0.037	−0.575	−0.766	2.472	53?	
A-29X-5, 40	273.08	−0.376	−0.750				
A-29X-5, 117	273.62	−0.116	−0.168	−0.759	2.303		
A-29X-6, 40	274.18	0.032	−0.219	−1.013	2.522		
A-29X-6, 106	274.84	0.032	−0.178				
A-30X-1, 88	279.18	0.191	−0.436	−0.541	2.802		
A-30X-4, 109	280.84			−0.555	2.637		FAD
A-31X-3, 137	290.43	0.103	−0.227	−0.731	2.394		*G. carribianica*
A-31X-4, 125	291.31			−0.386	2.640		
B-31X-1, 81	294.51	0.229	−0.603				
B-31X-2, 86	295.76			−0.441	2.563		
B-31X-3, 89	296.12			−0.457	2.552		
B-31X-4, 92	297.03			−0.567	2.535		
B-31X-5, 114	298.05			−0.467	2.190		
A-32X-1, 116	298.66			−0.381	2.334		
A-32X-2, 129	299.76			−0.339	2.371		
A-32X-4, 100	302.27			−0.376	2.364		
A-32X-6, 95	304.93			−0.373	2.527		
A-33X-2, 130	308.63			−0.620	2.649		
A-33X-3, 105	309.83			−0.571	2.606		
A-33X-6, 105	313.80	−0.276	−0.117	−0.500	2.319		
B-33X-3, 59	315.61			−0.538	2.269		
A-34X-1, 18	316.684			−0.684	2.501		
A-35X-1, 40	321.90			−0.443	2.387		
A-35X-1, 126	322.53			−0.415	2.433		
A-35X-2, 42	323.01			−0.480	2.326		
A-35X-2, 104	323.18			−0.457	2.287		
B-35X-1, 116	323.81			−0.536	2.225		
A-35X-3, 105	324.32			−0.396	2.197		
B-35X-2, 120	324.71			−0.655	2.514		
A-35X-4, 53	324.92			−0.494	2.231		
A-35X-4, 94	325.33			−0.544	2.564		
A-36X-1, 120	327.50			−0.947	2.511		
A-36X-2, 39	327.89			−0.540	2.679		
A-36X-4, 108	330.54			−0.766	2.135		LAD
A-36X-6, 37	332.50			−0.695	2.430		*D. brouweri*
A-36X-7, 37	333.75			−0.769	2.383		
A-36X-7, 116	334.51			−0.843	2.654		
B-38X-1, 74	352.64			−0.243	2.495		
B-38X-2, 121	353.63			−0.377	2.572		
A-39X-1, 40	355.40			−0.430	2.553		
A-39X-1, 142	355.77			−0.324	2.408		
A-39X-2, 43	356.11			−0.324	2.541		
A-39X-2, 142	356.67			−0.416	2.822		
A-39X-3, 43	357.00			−0.442	2.762		
A-39X-3, 84	357.21	0.113	−0.279	−0.411	2.695		
A-39X-4, 41	357.55	0.016	−0.355	−0.438	2.664		
A-39X-4, 120	358.27			−0.501	2.647		
A-39X-5, 41	358.79			−0.588	2.318		
A-39X-5, 112	359.15			−0.587	2.230		
A-40X-1, 72	365.02	−0.602	−0.332				
A-40X-1, 131	365.58			−0.762	2.670		
A-40X-2, 76	365.78			−0.941	2.748		
A-40X-2, 131	366.20	−0.505	−0.198	−0.759	2.683		
A-40X-3, 67	366.39	−0.583	−0.022	−0.649	2.584		
A-40X-4, 70	367.26			−0.680	2.745		
A-40X-5, 40	367.83			−0.571	2.420		
A-40X-6, 48	369.16			−0.783	2.460		
A-40X-6, 128	369.94			−0.737	2.464		
A-40X-7, 33	370.49			−0.791	2.654		
A-40X-CC, 30	370.86			−0.496	2.654		
A-41X-3, 71	376.20			−0.992	2.415		
A-41X-4, 12	376.75			−0.604	2.656		
A-41X-6, 55	378.89			−0.657	2.357		
A-41X-CC, 40	379.37	−0.380	−0.349	−0.803	2.523		
B-41X-1, 41	381.41			−0.807	2.484		

transgressive stages means that during the lightening of isotopic ratio of surface water mass (amount of global ice sheet reduced), the bottom temperature was colder than glacial stage or the lightening of isotopic ratio of bottom water mass was delayed. The delays are counted for depth 50–80 cm whose corresponding duration is calculated to be 2500–4000 yr. The delays result in significant peaks of the difference of oxygen isotope ratio $\delta^{18}O_{B-P}$ between benthic $\delta^{18}O_B$ and planktonic $\delta^{18}O_P$ in the transgressive stages.

CARBON ISOTOPE STRATIGRAPHY

The carbon isotope values range from $-0.6‰$ to $0.7‰$ for planktonic $\delta^{13}C_P$ and from $-1.7‰$ to $-0.1‰$ for benthic $\delta^{13}C_B$ (Fig. 3, Table 1). The heavier values in planktonic $\delta^{13}C_P$ are consistent with the uptake of lighter carbon by the biological productivity in the surface water. The fluctuations of carbon isotope values for Stages 1–15 are $1.3‰$ for benthic and planktonic foraminifers, $\delta^{13}C_B$, and $\delta^{13}C_P$ (Fig. 4), the changes and fluctuations of carbon isotopes are similar between benthic and planktonic. Generally $\delta^{13}C_B$ and $\delta^{13}C_P$ have an inverse correlation with oxygen isotope values $\delta^{18}O_B$ and $\delta^{18}O_P$, however, the changes of $\delta^{18}O$ and $\delta^{13}C$ are different. While the $\delta^{18}O$ during transgressive stages decreases sharply, called "termination" (Broecker and vanDonk, 1970). The $\delta^{13}C$ increases gradually, in spite of the synchronized changes of $\delta^{13}C$ with that of $\delta^{18}O$ during regressive stages; a typical case can be found during the transgressive stages from Stages 12–11, 10–9, 8–7, and 6–5.

$\delta^{18}O$ of the seawater is controlled by the global ice volume correlated with eustatic sea level, and $\delta^{13}C$ is influenced by the degree of the biological uptake of light carbon from the dissolved ΣCO_2 in the ocean (e.g., Broecker and Peng, 1982). Heavier value of $\delta^{13}C$ corresponds to higher degree of the uptake and the smaller amount of ΣCO_2 in the ocean. The inverse correlation between $\delta^{18}O$ and $\delta^{13}C$ suggests that glacial stages with low sea level had larger amount of ΣCO_2, and interglacial stages with high sea level had smaller amount of ΣCO_2 in the ocean. Two processes have been proposed to explain the inverse relation between $\delta^{18}O_B$ and $\delta^{13}C_B$ (Broecker, 1982). One is accumulation of light carbon ^{12}C in the increased and decreased terrestrial biomass associated with humus in interglacial and glacial stages, respectively (Shackleton, 1977), and the other is accumulation and oxidation of light carbon in the "shelf" sediments including fluvial deltaic, lagoonal, alluvial fan, and mangrove swamp, which would respond to glacio-eustatic sea level change in transgressive and regressive stages, respectively (Niitsuma and Ku, 1977). The responses in the former case are thought of as more reversible and with shorter time constant during glacial-interglacial cycles, but in the latter case completely different processes, deposition and oxidation of "shelf" sediments, relate to the carbon isotopic change. The time constant for the deposition can be thought of as longer than that for oxidation, and the rate of accumulation of light carbon might be nearly constant during a transgression, and not affected by the rate of transgression. However, the rate of oxidation should be followed to the regression, because the exposed organic carbon under the atmosphere might be oxidized suddenly.

The different manner of the isotopic changes $\delta^{18}O$ and $\delta^{13}C$ in Site 723 agrees with the "shelf" sediment model, because of the different responses in the transgressive and regressive stages, and the changing rate of $\delta^{13}C$ is nearly constant during transgressive stages.

The difference in the carbon isotope of benthic and planktonic $\delta^{13}C_{B-P}$ decreases from $-1.6‰$ to $-0.1‰$ with depth (Fig. 3). The fluctuation of the benthic $\delta^{13}C_B$ above Stage 6 is greater than the planktonic $\delta^{13}C_P$, and the difference $\delta^{13}C_{B-P}$ changes periodically synchronized with the fluctuation of $\delta^{18}O_P$. The greater differences appeared in the glacial interval, Stage 2,

Stage 6, and Stage 12, and the differences in the interglacial interval, Stage 1 and Stage 5, are similar values to those below Stage 7 (Fig. 4).

Because the carbon isotopic values of benthic $\delta^{13}C_B$ and planktonic $\delta^{13}C_P$ fluctuated in a parallel manner, the isotopic values represent mainly changes of carbon isotope of the dissolved ΣCO_2 in the water mass. The fluctuations of difference between benthic and planktonic $\delta^{13}C_{B-P}$ might represent the local changes in the depth profile of the biogenic productivity and/or bottom water chemistry. For example, the heavier planktonic carbon isotopic values $\delta^{13}C_P$ appear in the glacial time compared with the benthic values $\delta^{13}C_B$, and the heavier carbon isotopic values in the surface water indicate higher depletion of light carbon by biological uptake from dissolved ΣCO_2 in the surface water, derived by upwelling.

RECONSTRUCTION OF UPWELLING HISTORY

The reconstruction of the upwelling history in the northwestern Indian Ocean was the primary object of the Neogene Package of ODP Leg 117. Site 723 is sitting in the center of the upwelling area and in the central part of the oxygen minimum zone, and also has high resolution data because of the high rate of sedimentation. In the following sections, we will discuss the history of the upwelling by combining isotope data, mentioned above, with other available data.

Available Data for Discussion

Many kinds of analyses and measurements have been carried out on the sedimentary sequence of the drilled cores from Site 723. In this discussion, we will concentrate mainly on the last 600 ka because of the availability of detailed data sets. The available data and their meaning are listed as follows.

1. Isotopic data.

$\delta^{18}O_P$: Oxygen isotope of planktonic foraminifer *Pulleniatina obliquiloculata*; global change of oxygen isotopic composition of seawater.

$\delta^{18}O_B$: Oxygen isotope of benthic foraminifer *Uvigerina excellens*.

$\delta^{18}O_{B-P}$: Difference between planktonic and benthic oxygen isotope value; bottom temperature at 800 m depth; indicator of the depth of thermocline.

$\delta^{13}C_P$: Carbon isotope of planktonic foraminifer *Pulleniatina obliquiloculata*.

$\delta^{13}C_B$: Carbon isotope of benthic foraminifer *Uvigerina excellens*; global change of carbon isotopic composition of dissolved ΣCO_2 in seawater.

$\delta^{13}C_{B-P}$: Difference between planktonic and benthic carbon isotope value; balance of upwelling-productivity in surface water mass.

2. Shipboard data, described in Prell, Niitsuma, et al. (1989).

Sus: Bulk magnetic susceptibility measured with 10 cm interval; content of terrigenous matter in the sediments.
$CaCO_3$: Calcium carbonate content measured with 75 cm interval (two measurements/section); content of calcareous fossils and detrital calcite.
C_{org}: Organic carbon content measured with 150 cm interval (one measurement/section); preserved organic carbon in the sediments.

3. Shore-based data.

L: Lightness of sediment color on core photograph measured with video densitometer; the gradations are ranged from

30 for extreme black part to 220 for extreme white part on the black and white photographs (Niitsuma, this volume).

Sed: Rate of sedimentation based on the oxygen isotope stratigraphy and SPECMAP time table (Imbrie et al., 1984).

Correlation Group

The available data are cyclic in their values, related to the glacial-interglacial climatic change (Fig. 4). In this discussion, we used oxygen isotope of planktonic $\delta^{18}O_P$ as an indicator of the glacial-interglacial climatic change and oxygen isotope stratigraphic stages for the description of glacial-interglacial cycle. At first, we divide the available data sets into positive and negative correlation groups with $\delta^{18}O_P$ which is larger (heavier) value in the glacial stage and smaller (lighter) value in the interglacial stage.

1. Positive correlation group, which has higher or larger values in the glacial stage: $\delta^{18}O_B$, Sus, L, and Sed.
2. Negative correlation group, which has higher or large values in the interglacial stage: $\delta^{13}C_P$, $\delta^{13}C_B$, $\delta^{18}O_{B-P}$, $CaCO_3$, and C_{org}.

The available data are shown in Figure 4; the vertical axes of all plots are selected as upward for interglacial and downward for glacial conditions.

Significant Correlation

These data have generally good correlations with each other and show glacial-interglacial cycles clearly, but also show complexity. Further detailed correlations were examined for these data sets with isotopic data and the correlations follow.

1. Organic carbon content, C_{org}.

The range of the organic carbon content is from 1% to 6%. The content increases in the interglacial stages. The values fluctuated in all stratigraphic intervals since Stage 14, 550 ka. The minimum values appear in the glacial stages, Stages 2, 4, 6, 8, 10, and 12. The fluctuation and phases generally match well with $\delta^{18}O_P$, and better matching is realized with $\delta^{18}O_{B-P}$ for Stages 6–14. The transgressive feature from Stage 2 to 1 and minimum at Stage 2 are rather similar to $\delta^{13}C_{B-P}$.

2. Magnetic susceptibility, Sus.

The range of the magnetic susceptibility is from 10 to 130 × 10^{-6} SI. The magnetic susceptibility is high in the glacial stages and low in the interglacial stages, and the fluctuation can be correlated with $\delta^{18}O_P$. The amplitude of the fluctuation decreases significantly before Stage 8, 250 ka. The feature of change in the amplitude of fluctuation can be also found in $\delta^{13}C_{B-P}$.

3. Calcium carbonate content, $CaCO_3$.

The range of the calcium carbonate content is from 40% to 70% The content increases in the interglacial stages and decreases in the glacial stages. The amplitude of the fluctuation decreases significantly before Stage 8, 250 ka. The change in the amplitude of the fluctuation is similar to that of magnetic susceptibility, Sus, and $\delta^{13}C_{B-P}$. The individual peaks and valleys of the graph are matched better with $\delta^{18}O_{B-P}$, especially transgressive features from Stage 2 to 1 and minimum at Stages 3–4.

4. Lightness of sediment color, L.

The range of the lightness of sediment color is from 50 to 110. The color density of cored sediments at Site 723 is the darkest of all Leg 117 sites (Niitsuma, this volume). The pattern of the lightness can be expressed as intercalations of the lighter layers with various higher values in dark background with the lightness of 50. The frequency of the intercalations increases in the glacial stages, Stages 2, 4, 6, 10, and 12; however, the general feature does not appear for Stages 7–9, but the fluctuation of the lightness correlates with $\delta^{18}O_{B-P}$.

5. Rate of sedimentation, Sed.

Oxygen isotope stratigraphy gave us an age model by using a standard time table. In the study, SPECMAP time table (Imbrie et al., 1984) is used for the calculation of rate of sedimentation. The calculated rate of sedimentation distinctly changed with the glacial-interglacial cycles. The rate in the glacial stages is significantly high, two to four times that of interglacial stages, especially since Stage 8. The changes of sedimentation rate correlate with $\delta^{13}C_B$ and Sus.

Indicator of Upwelling

The location of Site 723 is in the central part of present upwelling area, which is related to the transport of the surface seawater by the southwest monsoon in summer. The upwelling brings deep water mass to the sea surface. Because the thermocline is pushed upward by the upwelling, and Site 723 is located around the depth range of thermocline, the bottom temperature at Site 723 should be colder in the season of upwelling (Fig. 2). The sea surface temperature (SST) in summer also becomes significantly cool by the upwelling, 23°–24°C, almost the same as the winter SST in this area (Prell, Niitsuma, et al., 1989; Prell and Streeter, 1982; Prell and Hutson, 1979). The cooling range by upwelling is about 4°–6°C and the upwelling reduces the seasonal fluctuation of SST.

The measured difference of planktonic and benthic oxygen isotopes $\delta^{18}O_{B-P}$ has an amplitude more than 1‰ of which equivalent difference of temperature is 4°C. The corresponding salinity difference is 4‰, which is comparable to the influence of the influx of river water in the Bengal Bay (Duplessy, 1982). The $\delta^{18}O_{B-P}$ fluctuation suggests that the bottom temperature is warmer and/or the isotopic composition of bottom water is affected by fresh water influx in the glacial stage.

The lowering of the sea level in the glacial stage should result in the same sense of change for the $\delta^{18}O_{B-P}$ fluctuation; however, the measured temperature gradient is 0.8°C/100 m for the depth range from 330 to 800 m (Fig. 2), and the contribution of 100 m sea level change for the oxygen isotope is only 0.2‰.

SST for the last glacial maximum, Stage 2, has been estimated as almost the same as at present, because of cancelling of the global cooling by the weakened monsoonal upwelling, based on isotopic and faunal data (Prell and Hutson, 1979). These data suggest that the surface water is not the main cause of the $\delta^{18}O_{B-P}$ fluctuation but rather the bottom water.

The cooler temperature of bottom water in the interglacial stage indicated by the $\delta^{18}O_{B-P}$ fluctuation can be explained as the result of depth changes of the thermocline induced by the upwelling with the southwest monsoon. It means that $\delta^{18}O_{B-P}$ is a good indicator of the upwelling, and the larger differences indicate the stronger upwelling.

The upwelling indicator $\delta^{18}O_{B-P}$ is larger in the interglacial stages with large amplitudes of glacial-interglacial cycles for Stages 1–13 (Fig. 3). The amplitude of the fluctuations before Stage 13 decreases and the $\delta^{18}O_{B-P}$ is larger, which indicates stronger upwelling. The depth of the Stage 13 coincides with the top depth of the intensive gas expansion after coring.

The upwelling seawater contains nutrients which induce productivity of biomass in the surface water. The high productivity supplies organic carbon into the sediments in the upwelling

area. The relation between stronger upwelling and high organic carbon is consistent with the correlation of the organic carbon content C_{org} and upwelling indicator $\delta^{18}O_{B-P}$, i.e., higher C_{org} appears in the interglacial stages with strong upwelling.

The upwelling brings ΣCO_2 with lighter carbon isotope, and the planktonic and benthic carbon isotope values should be affected by the upwelling. The isotope ratio of the ΣCO_2 in the surface water mass is controlled by the balance of the upwelling and productivity. The difference of the planktonic and benthic carbon isotope $\delta^{13}C_{B-P}$ is large in the case that the biological uptake exceeds the supply of lighter ΣCO_2 by upwelling, and is small in the case that upwelling exceeds the biological uptake. Because the measured $\delta^{13}C_{B-P}$ is smaller in the interglacial stages, the supply of lighter ΣCO_2 is estimated to exceed the biological uptake by the stronger upwelling. The correlation suggests that we can use $\delta^{13}C_{B-P}$ also as an indicator of the upwelling. The glacial-interglacial cycles of the $\delta^{13}C_{B-P}$ were unclear for the interval from Stage 8 to 11. The reduction of the amplitude of fluctuation of $\delta^{13}C_{B-P}$ and its small value indicate that the proportion of the uptake for the biological productivity did not increase in the glacial stages, because of the low organic carbon content C_{org}. A similar trend can be found in the calcium carbonate content $CaCO_3$.

Magnetic Susceptibility and Terrigenous Matter

Oxygen isotope curve has positive correlation with susceptibility curve; the interglacial stage has low susceptibility values, and the glacial stage has high susceptibility values. The susceptibility is controlled by the total amount of magnetic minerals in the sample, and the magnetic minerals are thought of as terrigenous in origin. The fluctuation of the magnetic susceptibility indicates that the supply of magnetic minerals decreased in the interglacial stage. Because the strength of the monsoon is estimated to increase in the interglacial stage, based on both of the upwelling indicators $\delta^{18}O_{B-P}$ and $\delta^{13}C_{B-P}$, the supply of terrigenous matter decreased in the interglacial stage with strong southwest monsoon.

The southwest monsoon is the most favorable carrier for the eolian transportation of terrigenous matter from the desert in the Arabian Peninsula and North Africa to the Oman Margin. If the main part of terrigenous matter in the Oman Margin sediments was transported as eolian grains by the southwest monsoon, the flux of the terrigenous matter should increase in the interglacial stage with strong monsoon. However, the fluctuation of the susceptibility indicates that the content of the terrigenous matter decreased in the interglacial stage. The reverse relation can be explained only by the dilution of terrigenous matter with the biogenic products relating to the strong upwelling in the interglacial. In such case, the rate of sedimentation during interglacial stages should be higher than in the glacial stage; however, the rate of sedimentation in the interglacial stage is significantly lower than in glacial stage, as mentioned above. These sets of data suggest that the main part of the terrigenous matter in the Oman Margin sediments were not transported as eolian particles by southwest monsoon.

Another way to explain the fluctuation of the terrigenous matter is by the fluvial transportation. The fluvial transportation is capable of carrying the large amount of terrigenous matter from the land area to the continental margin, and the amount might be sensitive to the climatic condition of humid or arid. The lower sea level in the glacial stage should be also effective in increasing the supply of the terrigenous matter to the sedimentary basin on the continental slope.

The distinct contrast in the strength of magnetic susceptibility between glacial and interglacial stages started from oxygen Stage 7 or 8.

Monsoon and Aridity of the Arabian and North African Desert

The magnetic susceptibility data and isotopic upwelling indicators clearly suggest the increase in the supply of the terrigenous matter in the glacial stage. The layer-by-layer correlation indicates that the increase of the sediment supply is not a local phenomenon at Site 723 but also all over the Oman Margin, and that the absolute flux of the sediments increased in the glacial stage; the sediments have various facies which indicate the changeable circumstance of the sediment supply (Niitsuma, this volume). These data suggest that the large amount of terrigenous matter in the glacial stage is transported from the land area by the drainage systems.

Meteorological studies show that the southwest monsoon is induced by the strong ascending current on the Himalaya-Tibet high-mountainous area in summer, and the counter-current of the southwest monsoon develops the Tropical Easterly Jet from southeast Asia to north Africa (Hahn and Manabe, 1975; Barnett et al., 1989). The Easterly Jet is directly related to the high precipitation in southeast Asia and arid climate in north Africa and the Arabian Peninsula. Because the arid climate of the Arabian Peninsula is maintained by the strong monsoon today, the glacial stage with weak monsoon and weak upwelling had a more humid climate in the Arabian Peninsula. The relation agrees better with the fluvial origin of the sediments in the glacial stages.

Although Kutzbach (1986) mentioned that lake levels in Africa were low in the last glacial, based on the data of Butzer et al. (1972) and Street and Grove (1979), humid conditions in the last glacial stage have been reported from the lake sediments of the Dead Sea and Zeribar in the Middle East and Lake Mundafan in the Arabian Peninsula (Street and Grove, 1979). Lake deposition of the Lake Mundafan in the central part of the Arabian Peninsula were classified into Series A, B, and C based on their radiocarbon date and altitude, and their dates are 36–17 ka, 9–6 ka, and 15–11 ka, respectively. Generally, beds of Series A occupy high parts of the basin and beds of Series B and C occupy low parts (McClure, 1976). The humid records during glacial stage support the fluvial origin of the sediment supply in glacial stages.

History of the Upwelling

The detailed history of the upwelling can be reconstructed with the available data sets since Stage 15, 600 ka. The most useful upwelling indicator $\delta^{18}O_{B-P}$ related to the depth of thermocline indicates that the upwelling in the Oman Margin developed more strongly in the interglacial stages. The present glacial-interglacial cycle can be traced back to Stage 8, 250 ka, with the cyclic changes of the other upwelling indicator $\delta^{13}C_{B-P}$. The cycle upheld the arid-humid cycle of the Arabian and North African Desert, and large amounts of terrigenous input were supplied in the glacial stage.

For the interval from Stage 8 to 12, 250–450 ka, the upwelling indicator $\delta^{18}O_{B-P}$ was still signifying the distinct glacial-interglacial cycle, but the other upwelling indicator $\delta^{13}C_{B-P}$ did not show such distinct cyclicity.

For Stages 12–15, 450–600 ka, the glacial-interglacial cycles can be traced back, however, the value of $\delta^{18}O_{B-P}$ remained strong in the upwelling side, and the sediments contain high concentration of gas. $\delta^{13}C_{B-P}$ recovered the glacial-interglacial cyclicity as in present cycles. This interval corresponds to the increasing stage of the global ice sheet volume from the pre-glacial cycles with small amplitude of oxygen isotope fluctuation to present glacial-interglacial cycles. The situations of upwelling can be estimated as strong as in the interglacial stage of the

present cycles, with slightly weak upwelling in the glacial stage. The cyclic input of the fluvial sediments to present cycles cannot be estimated.

Before Stage 15, 600 ka, the available data are limited because of the incomplete core recovery of and gas expansion of the cored sediments. Based on the isotopic results, the situations of upwelling and climate for Stage 12 to 15 can be traced back to the late Pliocene. The difference of planktonic and benthic oxygen isotope $\delta^{18}O_{B-P}$ increases with depth (Fig. 3). Because the difference $\delta^{18}O_{B-P}$ is good indicator of strength of upwelling, as mentioned above, the much stronger upwelling can be estimated in the late Pliocene to early Pleistocene time. The difference of carbon isotope $\delta^{13}C_{B-P}$ also gradually lessens, which indicated the stronger upwelling. The strong upwelling indicated by isotopic results is consistent with the high organic carbon content (Fig. 3), existence of thin laminated sedimentary structures which are characteristic of the anoxic condition under the high productive area of upwelling, and high content of gas in the sediments, which causes poor recovery of cored sediments and disturbance by gas expansion (Prell, Niitsuma, et al., 1989).

SUMMARY AND CONCLUSION

This paper mentions the results of isotopic measurements on the sedimentary sequence of Site 723, and discusses the history of the upwelling in the Oman Margin and paleoclimatology, related to the southwest monsoon in the northwestern Indian Ocean.

Site 723 is located in the center of mid-slope basin of the Oman margin, and high resolution data are available because of the high rate of sedimentation. The water depth of 808 m is situated on the center of the oxygen minimum zone developing under the upwelling area and on the middle part of the thermocline.

Oxygen isotope curves of planktonic $\delta^{18}O_P$ and benthic $\delta^{18}O_B$ can be correlated well with standard curves and can be traced back continuously to Stage 23 with high resolution measurements. The tentative correlation has been tried to Stage 53. The amplitudes of the fluctuations of the benthic $\delta^{18}O_B$ curve are significantly small, especially older than Stage 16, compared with planktonic $\delta^{18}O_P$.

Significant delays of benthic oxygen isotopes $\delta^{18}O_B$ appear in the transgressive stage from the planktonic $\delta^{18}O_P$. The delays are counted for depth 50–80 cm whose corresponding duration is calculated to be 2500–4000 yr.

Generally, carbon isotopes of benthic $\delta^{13}C_B$ and planktonic $\delta^{13}C_P$ have inverse correlation with oxygen isotope values $\delta^{18}O_B$ and $\delta^{18}O_P$, however, the changes of $\delta^{13}C$ are more gradual than those of $\delta^{18}O$ during transgressive stages in spite of the synchronized changes of $\delta^{13}C$ with those of $\delta^{18}O$ during regressive stages, which is agreeable with the "shelf" model for global carbon isotope fluctuation in the deep water mass.

The difference of oxygen isotope $\delta^{18}O_{B-P}$ indicates that the bottom temperature was warmer in the glacial stage than in the interglacial stage. The relation can be explained by the pushed-up thermocline during the strong upwelling stage in the interglacial stages. It means that $\delta^{18}O_{B-P}$ is a good indicator of the upwelling, and the larger differences indicate the stronger upwelling in the interglacial stages.

The difference of carbon isotope $\delta^{13}C_{B-P}$ also can be used as an indicator of the upwelling, because the smaller values of $\delta^{13}C_{B-P}$ appear in the interglacial stages with stronger upwelling estimated by $\delta^{18}O_{B-P}$, and the small values mean that upwelling ΣCO_2 exceeds the biological uptake.

The organic carbon content C_{org} is correlated with isotopic upwelling indicators $\delta^{18}O_{B-P}$ and $\delta^{13}C_{B-P}$, i.e., higher C_{org} appears in the interglacial stages with strong upwelling.

The calculated rate of sedimentation based on oxygen isotope stratigraphy in glacial stages is significantly high, two to four times that of interglacial stages. The isotopic upwelling indicators and the layer-by-layer correlation and magnetic susceptibility data show that the absolute flux of terrigenous matter and variability of lithofacies increased in the glacial stage. The terrigenous matter in the glacial stage is estimated to be transported from humid Arabian Peninsula under weak condition of Tropical Easterly Jet.

The present glacial-interglacial cycle with upwelling fluctuation and arid-humid alternation can be traced back to Stage 8, 250 ka. For the interval from Stage 8 to 12, 250–450 ka, the upwelling indicator $\delta^{18}O_{B-P}$ still observed the distinct glacial-interglacial cycle, but the other upwelling indicator $\delta^{13}C_{B-P}$ did not show such distinct cyclicity.

For Stages 12–15, 450–600 ka, the upwelling can be estimated as strong as in the interglacial stage of the present cycles, with slightly weak upwelling in the glacial stage. This upwelling and climate can be traced back to the late Pliocene. The strongest upwelling can be estimated in the late Pliocene to early Pleistocene by the isotopic indicators and the high organic carbon content.

REFERENCES

Barnett, T. P., Dumenil, L., Schlese, U., Roeckner, E., and Latif, M., 1989. The effect of Eurasian snow cover on regional and global climate variations. *J. Atmos. Sci.*, 46:661–668.

Broecker, W. S., 1982. Ocean chemistry during glacial time. *Geochim. Cosmochim. Acta*, 46:1689–1705.

Broecker, W. S., and Peng, T.-H., 1982. *Tracers in the Sea*: Palisades, NY (Eldigio Press).

Broecker, W. S., and vanDonk, J., 1970. Insolation changes, ice volumes, and the O^{18} record in deep-sea cores. *Rev. Geophys. Space Phys.*, 8:169–198.

Butzer, K. W., Isaac, G. L., Richardson, J. A., and Washbourn-Kamau, C., 1972. Radiocarbon dating of East African lake levels. *Science*, 175:1069–1076.

Craig, H., 1957. Isotopic standards for carbon and oxygen correction factors for mass spectrometric analysis of carbon dioxide. *Geochim. Cosmochim. Acta*, 12:133–149.

Duplessy, J. C., 1982. Glacial to interglacial contrasts in the northern Indian Ocean. *Nature*, 295:494–498.

Hahn, D. G., and Manabe, S., 1975. The role of mountains in the South Asian monsoon circulation. *J. Atmos. Sci.*, 32:1515–1541.

Imbrie, J., Hays, J. D., Martinson, D. G., McIntyre, A., Mix, A. C., Morley, J. J., Pisias, N. G., Prell, W. L., and Shackleton, N. J., 1984. The orbital theory of Pleistocene climate: support from a revised chronology of the marine $\delta^{18}O$ record. *In* Berger, A., Imbrie, J., Hays, J., Kukla, G., and Saltzman, B. (Eds.), *Milankovitch and Climate* (Pt. 1): Dordrecht (D. Reidel), 269–305.

Kahn, M. I., 1979. Non-equilibrium oxygen and carbon isotopic fractionation in tests of living planktonic foraminifera. *Oceanol. Acta*, 2:195–208.

Kutzbach, J. E., 1986. The changing pulse of the Monsoon. *In* Fein, J. S., and Stephens, P. L. (Eds.), *Monsoons:* New York (Wiley), 247–268.

McClure, H. A., 1976. Radiocarbon chronology of the Quaternary lakes in the Arabian Desert. *Nature,* 263:755–756.

Niitsuma, N., and Ku, T. L., 1977. What happened during geomagnetic reversals? *Kagaku,* 47:671–678.

Prell, W. L., and Hutson, W. H., 1979. Zonal temperature-anomaly maps of Indian Ocean surface waters: modern and ice-age patterns. *Science,* 206:454–456.

Prell, W. L., Imbrie, J., Martinson, D. G., Morley, J. J., Pisias, N. G., Shackleton, N. J., and Streeter, H. F., 1986. Graphic correlation of oxygen isotope stratigraphy application to the late Quaternary. *Paleoceanography,* 1:137–162.

Prell, W. L., Niitsuma, N., et al., 1989. *Proc. ODP, Init. Repts.,* 117: College Station, TX (Ocean Drilling Program).

Prell, W. L., and Streeter, H. F., 1982. Temporal and spatial patterns of monsoonal upwelling along Arabia: a modern analogue for the in-terpretation of Quaternary SST anomalies. *J. Mar. Res.,* 40:143–155.

Shackleton, N. J., 1977. Tropical rainforest history and the equatorial Pacific carbonate dissolution cycles. *In* Anderson, N. R., and Mala-hoff, A. (Eds.), *The Fate of Fossil Fuel CO_2 in the Oceans:* New York (Plenum), 401–428.

Street, F. A., and Grove, A. T., 1979. Global maps of lake-level fluctuations since 30,000 yr B.P. *Quat. Res.,* 12:83–118.

Wada, H., Fujii, N., and Niitsuma, N., 1984. Analytical method of stable isotope for ultra-small amounts of carbon dioxide with MAT 250 mass-spectrometer. *Geosci. Repts. Shizuoka Univ.,* 10:103–112.

Williams, D. F., Thunnell, R. C., Tappa, E., Rio, D., and Raffi, I., 1988. Chronology of the Pleistocene oxygen-isotope record: 0–1.88 m.y.B.P. *Palaeogeogr., Palaeoclimatol., Palaeoecol.,* 64:221–240.